**SEVENTH FRAMEWORK PROGRAMME**
**THEME 3**
**ICT - INFORMATION AND COMMUNICATION TECHNOLOGIES**

| | |
|---|---|
| **Project acronym:** | AEOLUS |
| **Project full title:** | Distributed Control of Large-Scale Offshore Wind Farms |
| **Project reference:** | **224548** |
| **Start date:** | 1 May 2008 |
| **Duration:** | 36 months |

**Deliverable no.:** 1.5a
**Title:** Final maps of wind fields and mechanical loads and energy output

| | |
|---|---|
| **Contractual date of delivery:** | 30 April 2010 |
| **Actual date of delivery:** | 07 June 2010 |
| **Lead beneficiary of this deliverable:** | ECN |
| **Author(s):** | A.J. Brand, J.W. Wagenaar |
| **Participant(s):** | A.J. Brand, J.W. Wagenaar |
| **Work packages contributing to the deliverable:** | WP1 |
| **Nature:** | R+O |
| **Version:** | 1 |
| **Total number of pages:** | 38 |
| **Dissemination level:** | PU |

**Summary:**
Quasi-steady maps of wind, loads and energy are presented for the ECN Wind turbine Test site Wieringermeer EWTW and the ECN Scale Wind Farm ESWF. These maps include tables with mean and standard deviation of six quantities (wind speed at the turbine, rotor thrust, tower bending moment, blade bending moment, aerodynamic power, and rotor shaft torque) and three short-term load quantifiers (equivalent tower bending moment, equivalent blade bending moment, and equivalent rotor shaft torque) as a function of three input quantities (wind speed, wind speed standard deviation, and wind direction). In addition the quasi-steady flow wind farm flow model and the computer programme that allows one to calculate these tables are presented. For the EWTW a comparison with measured data and a demonstration of power and load quantifiers are presented. It is concluded that differences between measurement and prediction are smaller than 2 m/s (wind speed) and 200 kW (power), measured minimum in wind speed and aerodynamic power at second or third turbine is not predicted, and main differences originate from unmodelled spatial variations in wind speed and too gradually modelled decay of wind speed. For the ESWF predicted data are presented.

# Final maps of wind fields and mechanical loads and energy output Part 1: Quasi-steady wind farm flow model - Model description

A.J. Brand and J.W. Wagenaar
26 May 2010
Final

## Abstract

Quasi-steady maps of wind, loads and energy are presented for the ECN Wind turbine Test site Wieringermeer EWTW and the ECN Scale Wind Farm ESWF. These maps include tables with mean and standard deviation of six quantities (wind speed at the turbine, rotor thrust, tower bending moment, blade bending moment, aerodynamic power, and rotor shaft torque) and three short-term load quantifiers (equivalent tower bending moment, equivalent blade bending moment, and equivalent rotor shaft torque) as a function of three input quantities (wind speed, wind speed standard deviation, and wind direction). In addition the quasi-steady flow wind farm flow model and the computer programme that allows one to calculate these tables are presented. For the EWTW a comparison with measured data and a demonstration of power and load quantifiers are presented. It is concluded that differences between measurement and prediction are smaller than 2 m/s (wind speed) and 200 kW (power), measured minimum in wind speed and aerodynamic power at second or third turbine is not predicted, and main differences originate from un-modelled spatial variations in wind speed and too gradually modelled decay of wind speed. For the ESWF predicted data are presented.

## Contents

# 1 Introduction

Specific objective of Work Package 1 of the FP7 project Aeolus is to develop quasi-static flow models which relate single turbine production and loading to a map of wind speeds. In this context the work in Task 1.3 "Improved flow model" was aimed at further investigating the largest discrepancies between the flow model developed in Task 1.2 and measurements in the ECN Scale Wind Farm ESWF, and at improving the flow model presented in Deliverable 1.3 on the base of new insights from these experiments. More specific, the objective of Task 1.3 is to derive energy production and fatigue loads for the ESWF from the flow field (Deliverable D1.4). Subsequently, Task 1.4 "Final flow and load/power relation" is aimed at calculating expected energy production and fatigue loads on base of the improved flow model.

Deliverable D1.3 presented 1) preliminary maps of wind, loads and energy for the ECN Wind turbine Test site Wieringermeer EWTW, and 2) the wind farm flow model that was developed for that purpose. In addition D1.3 presented a comparison with measured information, and a list with modelling issues. In Task 1.3 improvements in the flow model originated from re-analyzing the EWTW data, but unfortunately not from the ESWF data because the ESWF has not produced reliable data by the end of the reporting period.

This report presents 1) final maps of wind, loads and energy for the EWTW, 2) initial maps for the ESWF, and 3) the wind farm flow model. Together with the user's manual (Brand, 2010) it forms Deliverable D1.5. First, in chapter 2 the wind farm flow model is addressed. Next, in chapter 3 we present the final maps for the EWTW and a comparison to measured information, as well as preliminary maps for the ESWF. Finally, in chapter 4 we present a summary and outlook.

# 2 Quasi steady wind farm flow model

## 2.1 Outline

The quasi-steady wind farm model allows one to calculate maps of wind, loads and energy, or to be more specific the wind speed at each turbine in a wind farm plus the tower bending moment, the blade bending moment, the rotor shaft torque, the rotor thrust and the aerodynamic power of each turbine as a function of "ambient" wind speed, wind direction and turbulence intensity. Apart from the mean also the standard deviation a quantity is calculated. In addition the model calculates short-term load quantifiers for tower bending moment, blade bending moment and rotor shaft torque based on the concept of equivalent load.

In this section the structure of the flow model is presented. First the single wind turbine is addressed. In section 2.2 it is explained how by using momentum theory the aerodynamic state of a wind turbine is expressed in terms of an axial induction factor. Relations for mean and standard deviation of the axial induction factor are presented which both bring the effect of turbulence into account. Subsequently section 2.3 addresses tower bending moment, blade bending moment, rotor shaft torque, aerodynamic power, rotor thrust and short-term load quantifiers. Next, in section 2.4 relations for velocity deficit and extra turbulence due to a single wind turbine are introduced. We then proceed in section 2.5 with a cluster of wind turbines, and explain how streamwise and spanwise distance downstream each wind turbine are determined for a given wind direction. And we end in section 2.6 with a pointer to the user's manual of the quasi-steady wind farm flow model.

## 2.2 Wind turbine state

In this section we express the aerodynamic state of a wind turbine in terms of mean and standard deviation of the axial induction factor. The flow diagram is shown in figure 1, and the procedure is illustrated in figure 2.

Consider a wind turbine with rotor radius R that operates at hub-height wind speed U and rotor speed $\Omega(U)$. Then the tip speed ratio $\lambda$ is defined as:

$$\lambda(U) \equiv \frac{\Omega(U)R}{U}.$$

Now we assume that over a relatively short time period (of several seconds to several minutes) wind speed at hub height has a normal distribution with mean $\mu_U$ and standard deviation $\sigma_U$:

$$U : N(\mu_U, \sigma_U).$$

Note the ratio $\sigma_U/\mu_U$ defines the turbulence intensity.

Realizing that $\lambda$ is a function of one variable U, by using the expansions in appendix A.1 it can be shown that tip speed ratio approximately has a normal distribution with mean $\mu_\lambda$ and standard deviation $\sigma_\lambda$:

$$\mu_\lambda = \frac{\Omega R}{\mu_U}\left[1 + \frac{\sigma_U^2}{\mu_U^2}\right] \text{ and } \sigma_\lambda^2 = \left(\frac{\Omega R}{\mu_U}\right)^2\left[1 + 2\frac{\sigma_U^2}{\mu_U^2}\right]\frac{\sigma_U^2}{\mu_U^2}.$$

This is illustrated in figure 2. Next we consider the thrust curve of the wind turbine, which relates tip speed ratio $\lambda$ to thrust coefficient $C_T$. (Thrust essentially is aerodynamic force on the rotor.) Since the thrust curve generally depends on blade pitch angle $\theta$, as illustrated in figure 3, all possible turbine states can be represented by a set of thrust curves. Because of turbine control only a subset of states can be realized, which collectively define the effective thrust curve.

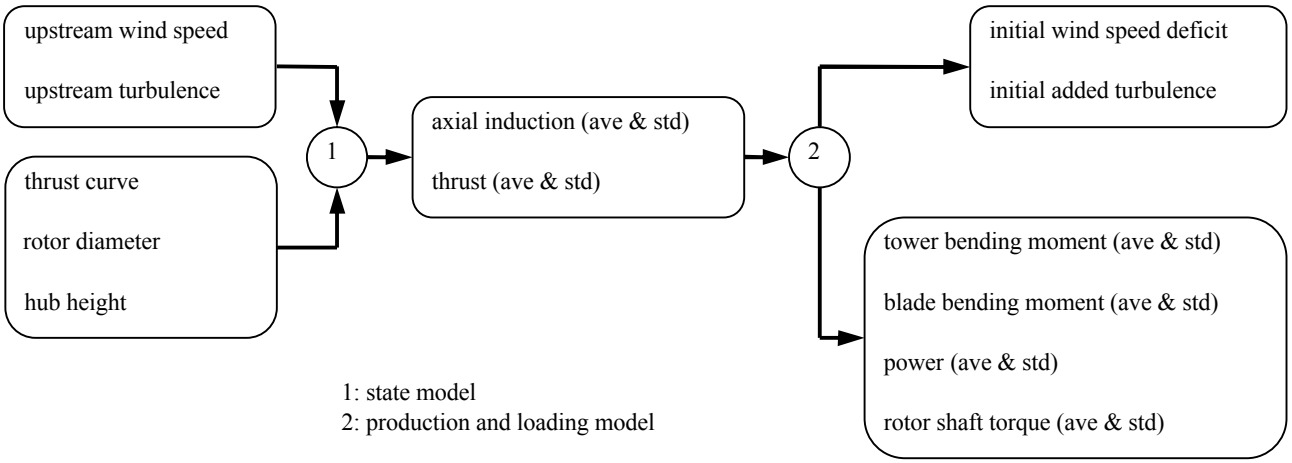


Figure 1 *Flow chart of the turbine model*

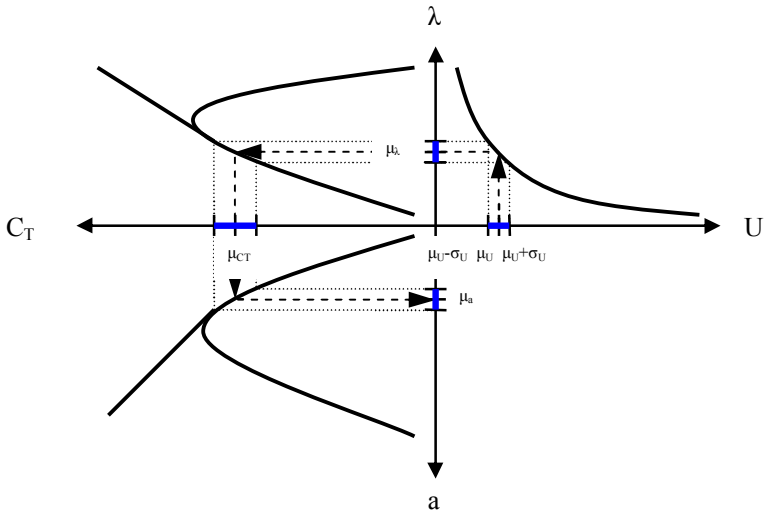


Figure 2 *Illustration of the procedure to express the state of a wind turbine in terms of the mean and the standard deviation of the axial induction factor a on basis of the mean and the standard deviation of the wind speed U. Mean and standard deviation are indicated by μ and σ, respectively; λ is the tip-speed ratio and $C_T$ is the thrust coefficient*

We represent the effective thrust curve and its first and second derivative in the form of a look-up table,

$$C_T\big|_{\lambda,\theta},\ \left.\frac{dC_T}{d\lambda}\right|_{\lambda,\theta} \text{ and } \left.\frac{d^2C_T}{d\lambda^2}\right|_{\lambda,\theta},$$

and calculate intermediate values by linear interpolation. Given the normally distributed tip speed ratio, by using the expansions in appendix A.1 it can be shown that the thrust coefficient has an approximate normal distribution with mean $\mu_{CT}$ and standard deviation $\sigma_{CT}$ (figure 2):

$$\mu_{C_T} \approx C_T(\mu_\lambda,\theta)+\frac{1}{2}\sigma_\lambda^2\left.\frac{d^2C_T}{d\lambda^2}\right|_{\mu_\lambda,\theta} \text{ and } \sigma_{C_T}^2 \approx \sigma_\lambda^2\left[\left(\left.\frac{dC_T}{d\lambda}\right|_{\mu_\lambda,\theta}\right)^2+\frac{1}{2}\sigma_\lambda^2\left(\left.\frac{d^2C_T}{d\lambda^2}\right|_{\mu_\lambda,\theta}\right)^2\right].$$

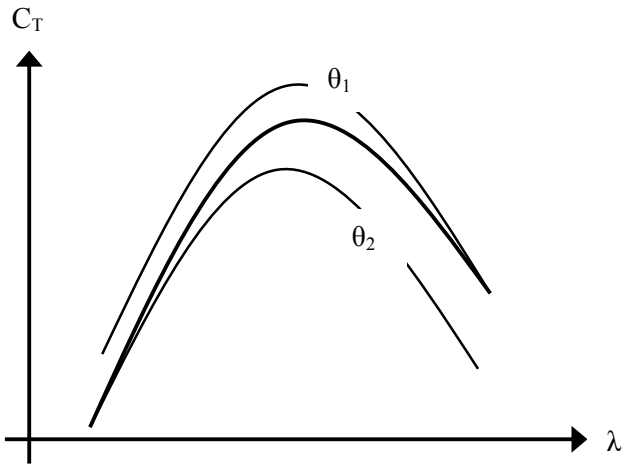


Figure 3 *Thrust curves for different values of the blade pitch angle θ and the effective thrust curve which results from turbine control. A thrust curve gives thrust coefficient $C_T$ as a function of tip-speed ratio λ*

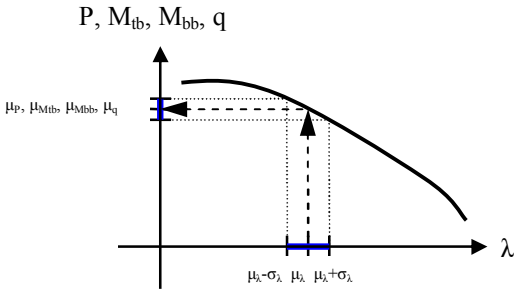


Figure 4 *Illustration of the procedure to express mean and standard deviation of power P, tower bending moment $M_{tb}$, blade bending moment $M_{bb}$ or rotor shaft torque q of a wind turbine in terms of the mean and the standard deviation of the tip-speed ratio λ*

Finally, we consider axial induction factor a, which quantifies velocity deficit in the rotor disc. According to momentum theory axial induction factor is a function of thrust coefficient:

$$a(\lambda,\theta)=\frac{1}{2}-\frac{1}{2}\sqrt{1-C_T(\lambda,\theta)}\,.$$

Given the normally distributed thrust coefficient, in a similar way it can be shown that axial induction factor has an approximate normal distribution with mean $\mu_a$ and standard deviation $\sigma_a$ (figure 2):

$$\mu_a \approx a(\mu_\lambda,\theta)+\frac{1}{2}\sigma_\lambda^2\left.\frac{d^2a}{d\lambda^2}\right|_{\mu_\lambda,\theta} \quad \text{and} \quad \sigma_a^2 \approx \sigma_\lambda^2\left[\left(\left.\frac{da}{d\lambda}\right|_{\mu_\lambda,\theta}\right)^2+\frac{1}{2}\sigma_\lambda^2\left(\left.\frac{d^2a}{d\lambda^2}\right|_{\mu_\lambda,\theta}\right)^2\right].$$

## 2.3 Wind turbine production and loading

### *2.3.1 Overview*

As to production and loading of a wind turbine we consider tower bending moment, blade bending moment, aerodynamic power and rotor shaft torque. In this section we express mean and standard deviation of such a quantity in terms of mean and standard deviation of axial induction factor. The procedure is illustrated in figure 1.

### *2.3.2 Tower bending moment*

Tower bending moment is the sum of the moments due to aerodynamic force on the rotor, aerodynamic force on the tower, and eccentricity of the nacelle.

First we consider aerodynamic force on the rotor, that is thrust. If a wind turbine with rotor diameter D operates at thrust coefficient $C_T$ and hub-height wind speed U, thrust T is:

$$T = \frac{\pi D^2 \rho}{8} C_T U^2 .$$

If hub height of the wind turbine is H, bending moment due to thrust is given by:

$$M_{tt} = TH . \quad (1)$$

Next we consider aerodynamic force on the rotor. At height h aerodynamic force $dF_{tow}$ on the segment dh of the tower is:

$$dF_{tow} = \frac{1}{2}\rho u^2(h) C_{drag} d \, dh ,$$

where u(h) is wind speed at h, $C_{drag}$ is drag coefficient of the tower and d is diameter of the tower. By assuming a power law wind speed profile with power 1/7, it follows that bending moment $M_{ta}$ due to force on the tower is:

$$M_{ta} = \frac{7}{32}\rho U^2 C_{drag} d H^2 . \quad (2)$$

Finally, we consider eccentricity of the nacelle. If the nacelle (including hub and rotor) is eccentric with respect to the tower axis, the corresponding moment $M_{te}$ is

$$M_{te} = (H \tan\varphi + d_{ecc}) m_{nac} g , \quad (3)$$

where φ is deflection of the tower, $d_{ecc}$ is eccentricity of the nacelle, $m_{nac}$ is total mass of the nacelle, and g is acceleration of gravity.

Tower bending moment $M_{tb}$ is the vector sum of the moments due to thrust on the rotor (equation 1), aerodynamic force on the tower (equation 2), and eccentricity of the nacelle (equation 3):

$$M_{tb} = M_{tt} + M_{ta} + M_{te} . \quad (4)$$

Realizing that wind speed at hub height is inversely proportional to tip-speed ratio and that thrust coefficient depends on tip-speed ratio, equation 4 expresses tower bending moment $M_{tb}$ as a function of tip-speed ratio λ. We represent this tower bending moment curve and its first and second derivative in the form of a look-up table,

$$M_{tb}|_\lambda , \left.\frac{dM_{tb}}{d\lambda}\right|_\lambda \text{ and } \left.\frac{d^2 M_{tb}}{d\lambda^2}\right|_\lambda ,$$

and calculate intermediate values by linear interpolation.

Under the assumption that hub-height wind speed $U:N(\mu_U,\sigma_U)$, in section 2.2 it has been shown that also tip speed ratio $\lambda:N(\mu_\lambda,\sigma_\lambda)$. Given normally distributed tip speed ratio, by using the expansions in appendix A.1 it can be shown that tower bending moment has an approximate normal distribution with mean $\mu_{Mtb}$ and standard deviation $\sigma_{Mtb}$ (see figure 4 for an illustration):

$$\mu_{Mtb} \approx M_{tb}(\mu_\lambda) + \frac{1}{2}\sigma_\lambda^2 \left.\frac{d^2 M_{tb}}{d\lambda^2}\right|_{\mu_\lambda} \quad \text{and} \quad \sigma_{Mtb}^2 \approx \sigma_\lambda^2 \left[ \left( \left.\frac{dM_{tb}}{d\lambda}\right|_{\mu_\lambda} \right)^2 + \frac{1}{2}\sigma_\lambda^2 \left( \left.\frac{d^2 M_{tb}}{d\lambda^2}\right|_{\mu_\lambda} \right)^2 \right].$$

### *2.3.3 Blade bending moment*

Blade bending moment originates from axial force on the rotor blade and tangential force due to gravity.

In appendix B it is shown that at a first approximation axial force $F_b$ on a rotor blade depends as follows on axial induction factor a and tip speed ratio $\lambda$:

$$F_b \approx \frac{\pi \rho \Omega^2 D^4}{4 N_b} \frac{a(1-a)}{\lambda^2}, \tag{5}$$

where $\rho$ is air density, $\Omega$ rotor speed, D rotor diameter, and $N_b$ the number of rotor blades.

If $m_{blade}$ is mass of the blade and g is acceleration of gravity, tangential force $F_g$ on the blade due to gravity is

$$F_g = m_{blade} g \cos\phi, \tag{6}$$

where ø is the rotor azimuth angle.

Given that $F_b$ acts on 2/3 of the blade length (e.g. Manwell et. al, 2002, section 4.3.1.2) and that centre of mass is at 5/12 of the blade length, blade bending moment vector $M_{bb}$ is:

$$\underline{M}_{bb} = \left( \frac{1}{3} F_b D, \frac{5}{24} F_g D \right),$$

with $F_b$ and $F_g$ according to equations 5 and 6. By averaging over a cycle it can be shown that effective blade bending moment $M_{bb,eff}$ is given by

$$M_{bb,eff}^2 \equiv \left|\underline{M}_{bb}\right|^2 = \left( \frac{1}{9} F_b^2 + \frac{25}{1152} m_{blade}^2 g^2 \right) D^2. \tag{7}$$

Equation 7 constitutes the blade bending moment curve, which we together with its first and second derivative express in the form of a look-up table,

$$M_{bb}|_\lambda, \quad \left.\frac{dM_{bb}}{d\lambda}\right|_\lambda \quad \text{and} \quad \left.\frac{d^2 M_{bb}}{d\lambda^2}\right|_\lambda.$$

Under the assumptions described in section 2.3.1 blade bending moment has an approximate normal distribution with mean $\mu_{Mbb}$ and standard deviation $\sigma_{Mbb}$:

$$\mu_{Mbb} \approx M_{bb}(\mu_\lambda) + \frac{1}{2}\sigma_\lambda^2 \left.\frac{d^2 M_{bb}}{d\lambda^2}\right|_{\mu_\lambda} \quad \text{and} \quad \sigma_{Mbb}^2 \approx \sigma_\lambda^2 \left[ \left( \left.\frac{dM_{bb}}{d\lambda}\right|_{\mu_\lambda} \right)^2 + \frac{1}{2}\sigma_\lambda^2 \left( \left.\frac{d^2 M_{bb}}{d\lambda^2}\right|_{\mu_\lambda} \right)^2 \right].$$

### 2.3.4 Power

According to momentum theory, power coefficient $C_P$ depends as follows on axial induction factor a:

$$C_P = 4a(1-a)^2 \text{ with } a = \frac{1}{2} - \frac{1}{2}\sqrt{1-C_T(\lambda)},$$

where $\lambda$ is tip-speed ratio. Power P is a function of power coefficient $C_P$ and hub-height wind speed U:

$$P = \frac{\pi D^2 \rho}{8} C_P U^3,$$

and for that reason depends on tip-speed ratio. Proceeding in a similar way as in section 2.3.1, we introduce a power curve and its first and second derivative in the form of a look-up table with tip-speed ratio as independent variable:

$$P|_\lambda, \left.\frac{dP}{d\lambda}\right|_\lambda \text{ and } \left.\frac{d^2P}{d\lambda^2}\right|_\lambda,$$

and conclude that power has an approximate normal distribution with mean $\mu_P$ and standard deviation $\sigma_P$:

$$\mu_P \approx P(\mu_\lambda) + \frac{1}{2}\sigma_\lambda^2 \left.\frac{d^2P}{d\lambda^2}\right|_{\mu_\lambda} \text{ and } \sigma_P^2 \approx \sigma_\lambda^2 \left[\left(\left.\frac{dP}{d\lambda}\right|_{\mu_\lambda}\right)^2 + \frac{1}{2}\sigma_\lambda^2 \left(\left.\frac{d^2P}{d\lambda^2}\right|_{\mu_\lambda}\right)^2\right].$$

### 2.3.5 Rotor shaft torque

Rotor shaft torque q is the ratio of aerodynamic power P and rotor speed $\Omega$:

$$q = \frac{P}{\Omega}.$$

On basis of the results of sub-section 2.3.3 it can be shown that mean $\mu_q$ and standard deviation $\sigma_q$ of the rotor shaft torque are:

$$\mu_q = \frac{\mu_P}{\Omega} \text{ and } \sigma_q = \frac{\sigma_P}{\Omega}.$$

### 2.3.6 Rotor thrust

Thrust T on the rotor is a function of thrust coefficient $C_T$ and hub-height wind speed U:

$$T = \frac{\pi D^2 \rho}{8} C_T U^2,$$

and for that reason depends on tip-speed ratio. We introduce the first and the second derivative in the form of a look-up table with tip-speed ratio as independent variable:

$$T|_\lambda, \left.\frac{dT}{d\lambda}\right|_\lambda \text{ and } \left.\frac{d^2T}{d\lambda^2}\right|_\lambda,$$

and conclude that thrust has an approximate normal distribution with mean $\mu_T$ and standard deviation $\sigma_T$:

$$\mu_T \approx T(\mu_\lambda) + \frac{1}{2}\sigma_\lambda^2 \left.\frac{d^2T}{d\lambda^2}\right|_{\mu_\lambda} \quad \text{and} \quad \sigma_P^2 \approx \sigma_\lambda^2 \left[ \left( \left.\frac{dT}{d\lambda}\right|_{\mu_\lambda} \right)^2 + \frac{1}{2}\sigma_\lambda^2 \left( \left.\frac{d^2T}{d\lambda^2}\right|_{\mu_\lambda} \right)^2 \right].$$

### *2.3.7 Short-term load quantifiers*

The quasi-steady wind farm flow model translates information on variations in the wind speed during periods of 10 minutes into information on variations in mechanical loads. Subsequently the model translates the information on load variation into a short-term load quantifier. In this section the approach is presented.

The load quantifier proposed in the short-term (in contrast to life-time) analysis of fatigue is equivalent load $L_{eq}$ of a series of loads $L_j$ (j = 1, 2, 3, …, N):

$$L_{eq}^m \equiv \frac{1}{N}\sum_i n_i L_i^m = \frac{1}{N}\sum_j L_j^m \;= \text{m-th raw moment of the observed loads.}$$

Here L indicates load, m is the slope of the SN-curve of the material and N is the number of load observations in the time period. Furthermore, $n_i$ is the number of loads with value $L_i$, and j indicates an individual load in the series $L_j$.

Note $L_{eq}$ is not equal to equivalent load range (e.g. Guidelines, 2001, page 80); future work is aimed at relating $L_{eq}$ to fatigue load.

If the load is a moment (e.g. tower bending moment, or blade bending moment), $n_i$ is the number of load observations of level $L_i$ in the time period, $N = \Sigma_i n_i$ is the number of load observations in that period, and m is 4 (steel tower) or 12 (GRP blade). (cf. Guidelines, 2001, page 80.)
If, on the other hand, the load is a shaft load (e.g. rotor shaft torque), $n_i$ is the number of revolutions at shaft load $L_i$, $N = \Sigma_i n_i$ is the number of revolutions, and m is 3. (cf. Guidelines, 2001, pages 136-137.)

Under the assumption that the observed loads $L_j$ are normally distributed with mean $\mu_L$ and standard deviation $\sigma_L$, their m-th raw moment, and for that reason the equivalent load, can be expressed in terms of $\mu_L$ and $\sigma_L$:

$$\frac{1}{N}\sum_j L_j^m = f(\mu_L, \sigma_L).$$

By using the definition of the m-th raw moment of the normally distributed variable $x:N(\mu_x,\sigma_x)$ (e.g. Abramowitz and Stegun, 1972, p. 928)

$$\mu_x^{(m)} \equiv \frac{1}{\sigma_x\sqrt{2\pi}} \int_{x=-\infty}^{\infty} x^m \exp\left\{ -\frac{1}{2}\left( \frac{x-\mu_x}{\sigma_x} \right)^2 \right\} dx ,$$

the binomial theorem for integer values of m (e,g, Abramowitz and Stegun, 1972, p. 10)

$$(a+b)^m = \sum_{k=0}^{m} \binom{m}{k} a^{m-k}\, b^k \quad \text{with} \quad \binom{m}{k} = \frac{m!}{k!\,(m-k)!}, \text{ and}$$

the analytical solution of the Gaussian integral for integer values of the order m (Weisstein, 2010)

$$\int_{x=0}^{\infty} x^m \exp\{-cx^2\}dx = \begin{cases} \dfrac{(m-1)!!}{2^{\frac{m}{2}+1} c^{\frac{m}{2}}}\sqrt{\dfrac{\pi}{c}} & \text{for n even} \\ \dfrac{((m-1)/2)!}{2c^{\frac{m+1}{2}}} & \text{for n odd} \end{cases},$$

it can be shown that equivalent loads relevant to shaft loads, tower bending moments and blade bending moments are:

(m= 3) $L_{eq} = \left(\mu_L^3 + 3\mu_L\sigma_L^2\right)^{\frac{1}{3}}$,

(m= 4) $L_{eq} = \left(\mu_L^4 + 6\mu_L^2\sigma_L^2 + 3\sigma_L^4\right)^{\frac{1}{4}}$,

(m= 12) $L_{eq} = \left(\mu_L^{12} + 66\mu_L^{10}\sigma_L^2 + 1485\mu_L^8\sigma_L^4 + 13860\mu_L^6\sigma_L^6 + 51975\mu_L^4\sigma_L^8 + 62370\mu_L^2\sigma_L^{10} + 10395\sigma_L^{12}\right)^{\frac{1}{12}}$.

The crucial assumption on the normal distribution of the loads is fair in a short-term fatigue assessment of wind turbine components because:

- In the short time period (10 minutes) the number of observations or revolutions is high (600 resp. ~200), and
- Under normal operation during a 10-minute period wind turbine loads have experimentally been found to be normally distributed with well defined mean and standard deviation.

In the approach it is further assumed that load mean $\mu_L$ as well as load standard deviation $\sigma_L$ depend on wind speed mean $\mu_U$ and wind speed standard deviation $\sigma_U$:

$$\mu_L = \mu_L(\mu_U, \sigma_U) \text{ and } \sigma_L = \sigma_L(\mu_U, \sigma_U).$$

This crucial assumption is motivated by experimental and modelling based identification of the parameters that influence equivalent loads (Dekker and Pierik, 1999, part 1, sub B, section 5.4), with as the conclusion that:

- The primary fatigue loading parameter is standard deviation of the longitudal wind speed component[1], and
- The equivalent load is a function of wind speed standard deviation $\sigma_U$ and, because at higher wind speeds a constant value of the turbulence intensity may be assumed, mean wind speed $\mu_U$.

## 2.4 Velocity deficit and extra turbulence due to a wind turbine

### *2.4.1 Velocity deficit*

In this sub-section we present the model for velocity deficit downstream of a wind turbine (figure 5). On basis of quite a large amount of experimental evidence (e.g. Barthelmie et al, 2003; Elliot, 1991; Milborrow, 1980) we model the velocity $\mu$ at position (r,x) in the wake of a single turbine as follows:

$$\mu(r,x) = \mu_0 - \Delta\mu(r,x).$$

Here $\mu_0$ is upstream velocity and $\Delta\mu$ is velocity deficit:

$$\frac{\Delta\mu(r,x)}{\Delta\mu_{ini}} = \left(\frac{x}{2D}\right)^n \exp\left\{-\alpha_1 \frac{r^2}{\beta^2(x)}\right\}$$

where

[1] The second important parameter is yaw misalignment, and the third important parameter is turbulence structure

$\Delta\mu_{ini} = 2a\mu_0$

$n = -1.04 \pm 0.07$ ,
$\alpha_1 = 0.693$ , and
$\frac{2\beta(x)}{D} = \gamma\left(\frac{x}{D}\right)^{\delta}$ with $\gamma = 0.3$ and $\delta = 0.63$ .

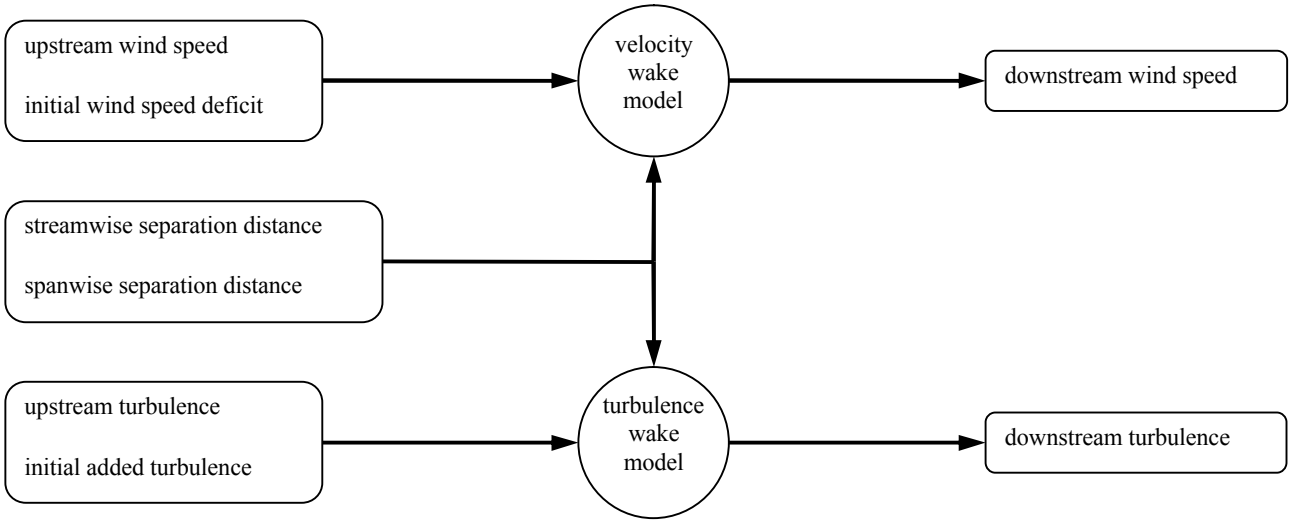


Figure 5 *Flow chart wake model*

Here $\Delta\mu_{ini}$ is the initial value of velocity deficit which is reached at a distance of two rotor diameters behind the wind turbine. According to momentum theory in the absence of turbulence initial velocity deficit has the value $2a\mu_0$ where a is the axial induction factor.

### *2.4.2 Added turbulence*

In this sub-section we present the model for turbulence downstream of a wind turbine (figure 5). On basis of the assumption that velocity is a stochastic process and experimental evidence (e.g. Elliot, 1991) we model turbulence in terms of velocity standard deviation σ. At position (r,x) in the wake of a single turbine velocity variance is the sum of upstream velocity variance $\sigma_0^2$ and velocity variance $\sigma^2_{add}$ added by the wind turbine:

$$\sigma^2(r,x) = \sigma_0^2 + \sigma^2_{add}(r,x).$$

Added variance $\sigma^2_{add}$ is the sum of two components, each originating from the production of turbulence at the edge of the rotor disc:

$$\sigma^2_{add}(r,x) = \sigma^2_{add,1}(r,x) + \sigma^2_{add,2}(r,x) \text{ with } \sigma_{add,1} = f_1(r,x)\,\sigma_{add,x}(x) \text{ and } \sigma_{add,2} = f_2(r,x)\,\sigma_{add,x}(x),$$

where $f_1(r,x)$ and $f_2(r,x)$ take care of decay of turbulence in spanwise direction r and $\sigma_{add,x}(x)$ takes care of decay in streamwise direction.

We model $\sigma_{add,x}$ with a power function:

$$\sigma^2_{add,x}(x) = \sigma^2_{add,ini}\left(\frac{x}{2D}\right)^m$$

where

$$\frac{\sigma_{add,ini}^2}{\mu_0^2} = c_{GCL} a \text{ with } c_{GCL} = 0.106, \text{ and } m = \frac{1-2a}{a(1-a)} \frac{n}{1+k}.$$

Here $\sigma_{add,ini}$ is initial added turbulence, which originates from thrust on the rotor as derived from the GCL model (Dekker and Pierik, 1998, Section 2.4.1). Power m depends on an energy redistribution fraction k, derived in appendix C.

We model $f_1(r,x)$ and $f_2(r,x)$ with an exponential function:

$$f_1(r,x) = \frac{1}{2} \exp\left\{ -\alpha_2 \left( \frac{r - R_1(x)}{R} \right)^2 \right\} \text{ and } f_2(r,x) = \frac{1}{2} \exp\left\{ -\alpha_2 \left( \frac{r + R_1(x)}{R} \right)^2 \right\},$$

where the $R_1(x)$ function causes the two peaks originating from the rotor disc edge to merge at a downstream position of eight rotor diameters:

$$\frac{R_1(x)}{R} = 1 \text{ if } 0 \le \frac{x}{D} < 2, \quad \frac{R_1(x)}{R} = \frac{1}{6}\left[ 8 - \frac{x}{D} \right] \text{ if } 2 \le \frac{x}{D} \le 8 \text{ or } \frac{R_1(x)}{R} = 0 \text{ if } \frac{x}{D} > 8.$$

The parameter $\alpha_2$ essentially sets the spanwise size of the region with added turbulence; with the value

$$\alpha_2 = \ln 100 / 4 \approx 1.15$$

added turbulence at one edge of the disc due to the other edge is minimal, and vice versa.

## 2.5 Cluster of wind turbines

In this section we determine the ranking of wind turbines in a cluster as a function of wind direction, and the distance in streamwise and in spanwise direction to another wind turbine (figure 6).

First the ranking of wind turbines in a cluster as a function of wind direction. To this end consider the wind direction φ (with respect to North or positive y-axis of the coordinate system) and introduce the wind front in the form of a line perpendicular to wind direction; see figure 7. Also introduce the angle β between the wind front and the positive x-axis:

$$\beta = \pi - \varphi.$$

Then it can be shown that the distance $d_i$ between the wind turbine at ($x_{Ti}$, $y_{Ti}$) and the front is:

$$d_i = \frac{x_{T_i} \tan\beta - y_{T_i}}{\sqrt{1 + \tan^2 \beta}}.$$

As to the ranking of the wind turbines we assume that the wind front travels through the cluster such that first the wind turbine with the smallest distance $d_i$ is reached, next the one with the second-smallest $d_i$ and so on until the wind turbine with the largest $d_i$.

The streamwise distance $s_1$ and the spanwise distance $s_2$ to a wind turbine at ($x_{Ti+1}$, $y_{Ti+1}$) as calculated from an "upstream" wind turbine at ($x_{Ti}$, $y_{Ti}$) are:

$$s_1 = s_x \cos\gamma \text{ and } s_2 = s_x \sin\gamma \text{ with } \gamma = -\frac{\pi}{2} - \varphi - \delta.$$

Here $s_x$ is the separation distance between the two wind turbines and δ is the corresponding separation angle:

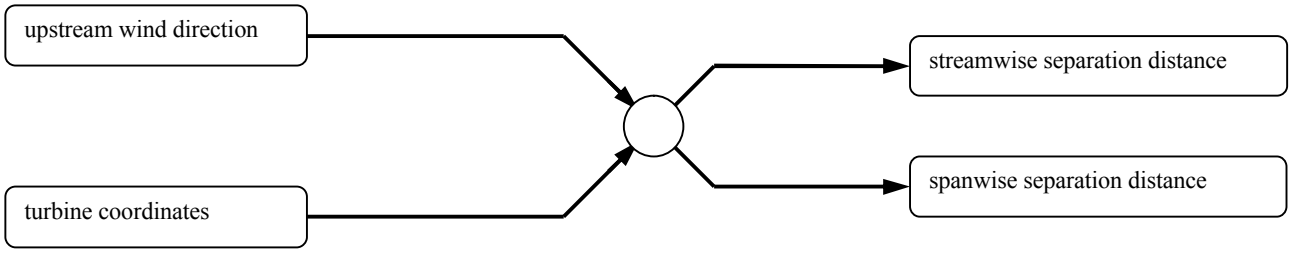


Figure 6 *Flow chart cluster model*

$$s_x^2 = \left(x_{T_{i+1}} - x_{T_i}\right)^2 + \left(y_{T_{i+1}} - y_{T_i}\right)^2 \text{ and } \tan\delta = \frac{y_{T_{i+1}} - y_{T_i}}{x_{T_{i+1}} - x_{T_i}}.$$

The velocity wake is handled by adding local velocity deficits (see sub-section 2.4.1) to the velocity field. As an example consider position P in the wake of two turbines. First the velocity deficit in P due to the most upstream turbine is calculated. Next the velocity deficit at the second turbine, the velocity at the second turbine and the initial velocity deficit behind the second turbine are determined (in that order). Then the velocity deficit in P due to the second turbine is calculated, and finally the two velocity deficits are added to the upstream velocity in order to obtain the velocity at point P.

The turbulence wake is handled in a similar way by adding local velocity variances (see sub-section 2.4.2) to the velocity variance field.

## 2.6 Code and user's manual

The wind farm model described in the sections 2.2 to 2.5 and shown in figure 8 has been coded in a Fortran programme. This programme requires as input:

- Number of wind turbines in the cluster and their (x,y) coordinates,
- Number of rotor blades of the turbine,
- Diameter of the turbine rotor
- Height of the turbine hub,
- Diameter of the tower,
- Mass of the nacelle plus rotor,
- Mass of a rotor blade,
- Eccentricity of the mass in the rotor plus hub,
- Effective thrust curve of the wind turbine,
- Rotor speed at cut-in, nominal and cut-out wind speed,
- Blade pitch angle at cut-in, nominal and cut-out wind speed,
- Ambient wind speed mean and standard deviation, and
- Ambient wind direction.

The output consists of mean and standard deviation of six wind, load and energy parameters:

- Wind speed,
- Tower bending moment,
- Blade bending moment,
- Rotor shaft torque,
- Rotor thrust, and
- Aerodynamic power;

two state parameters:

- Rotor speed, and
- Blade pitch angle;

plus three short-term load quantifiers:

- Equivalent tower bending moment,
- Equivalent blade bending moment, and
- Equivalent rotor shaft torque.

As an example table 1 shows an excerpt from the flow/load/energy map of the EWTW in the form of a "power curve". The user's manual (Brand, 2010) presents a more detailed description of the programme.

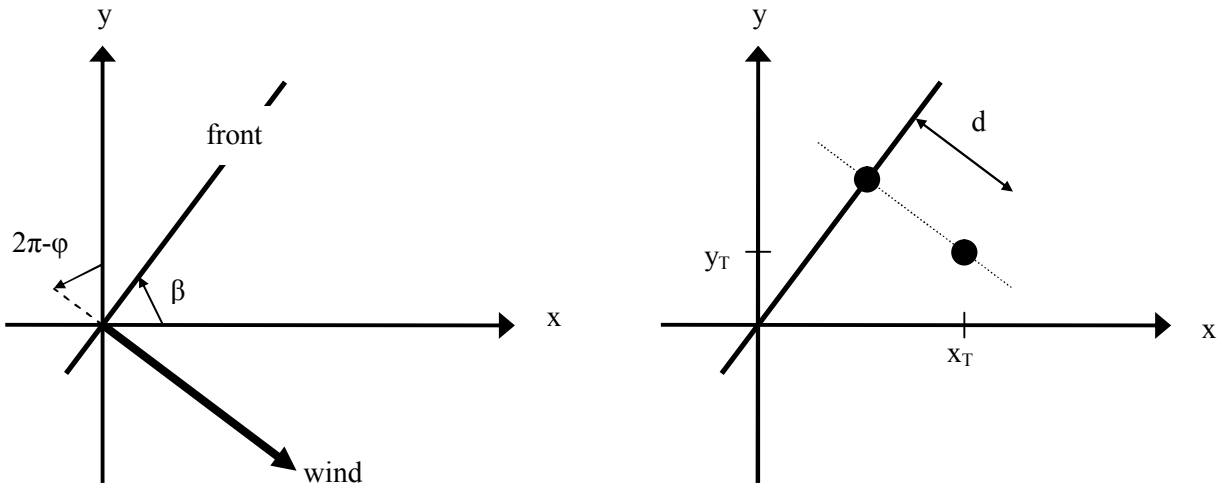


Figure 7 *Wind direction φ and angle β between the wind front and the positive x-axis (left) and distance d between the wind turbine at ($x_T$, $y_T$) and the wind front (right)*

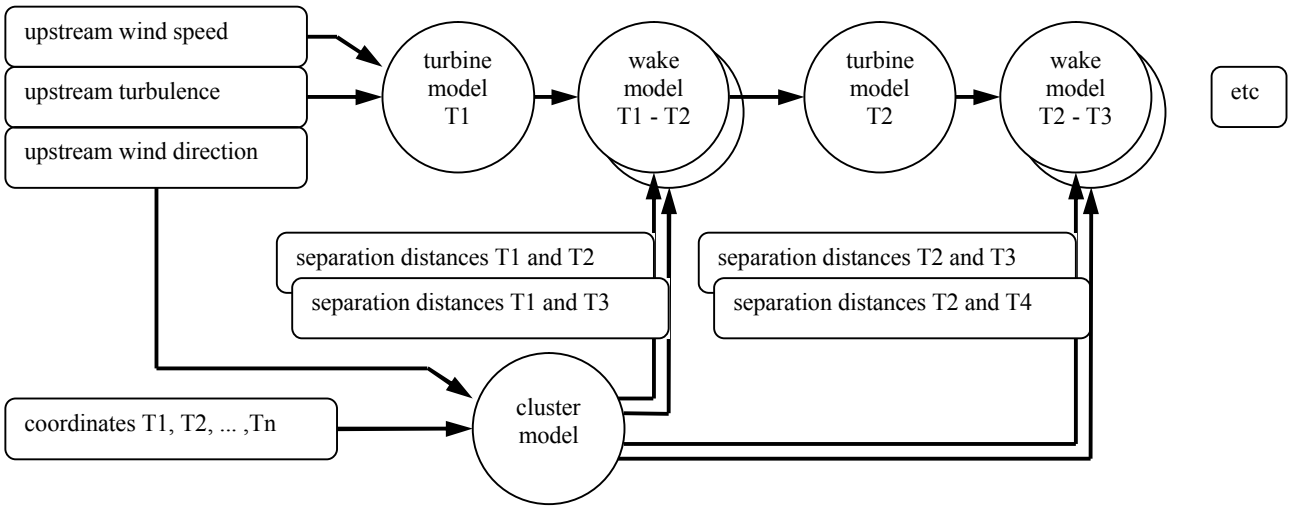


Figure 8 *Flow chart farm model*

Table 1 *Excerpt from the flow/load/energy map of the EWTW in the form of a "power curve"*

| wsave [m/s | wsstd [m/s | wdave [de | x [m] | | | y [m] | | | | wsaveloc | | | | | tbmomav | | | | bbmomav | | | | powave [ | | | | rstorqave | | | |
|---|---|---|---|---|---|---|---|---|---|---|---|---|---|---|---|---|---|---|---|---|---|---|---|---|---|---|---|---|---|---|
| 1 | 0.09 | 185 | 608.7 | 913 | 0 | 1217.4 | 304.3 | -53.3 | -79.9 | 0 | -106.5 | -26.6 | 1 | 1 | 1 | 1 | 1 | 0.00E+00 | 0.00E+00 | 0.00E+00 | 0.00E+00 | 0.00E+00 | 0.00E+00 | 0.00E+00 | 0.00E+00 | 0.00E+00 | 0.00E+00 | 0.00E+00 | 0.00E+00 | 0.00E+00 | 0.00E+00 | 0.00E+00 |
| 2 | 0.18 | 185 | 608.7 | 913 | 0 | 1217.4 | 304.3 | -53.3 | -79.9 | 0 | -106.5 | -26.6 | 2 | 2 | 2 | 2 | 2 | 0.00E+00 | 0.00E+00 | 0.00E+00 | 0.00E+00 | 0.00E+00 | 0.00E+00 | 0.00E+00 | 0.00E+00 | 0.00E+00 | 0.00E+00 | 0.00E+00 | 0.00E+00 | 0.00E+00 | 0.00E+00 | 0.00E+00 |
| 3 | 0.27 | 185 | 608.7 | 913 | 0 | 1217.4 | 304.3 | -53.3 | -79.9 | 0 | -106.5 | -26.6 | 3 | 3 | 3 | 3 | 3 | 0.00E+00 | 0.00E+00 | 0.00E+00 | 0.00E+00 | 0.00E+00 | 0.00E+00 | 0.00E+00 | 0.00E+00 | 0.00E+00 | 0.00E+00 | 0.00E+00 | 0.00E+00 | 0.00E+00 | 0.00E+00 | 0.00E+00 |
| 4 | 0.36 | 185 | 608.7 | 913 | 0 | 1217.4 | 304.3 | -53.3 | -79.9 | 0 | -106.5 | -26.6 | 4 | 4 | 4 | 4 | 4 | 2.65E+03 | 2.65E+03 | 2.65E+03 | 2.65E+03 | 2.65E+03 | 9.98E+02 | 9.98E+02 | 9.98E+02 | 9.98E+02 | 9.98E+02 | 1.38E+01 | 1.38E+01 | 1.38E+01 | 1.38E+01 | 1.17E+01 | 1.17E+01 | 1.17E+01 | 1.17E+01 | 1.17E+01 |
| 5 | 0.45 | 185 | 608.7 | 913 | 0 | 1217.4 | 304.3 | -53.3 | -79.9 | 0 | -106.5 | -26.6 | 5 | 5 | 5 | 5 | 5 | 4.47E+03 | 4.47E+03 | 4.47E+03 | 4.47E+03 | 4.47E+03 | 1.10E+03 | 1.10E+03 | 1.10E+03 | 1.10E+03 | 1.10E+03 | 1.17E+02 | 1.17E+02 | 1.17E+02 | 1.17E+02 | 1.17E+02 | 9.50E+01 | 9.50E+01 | 9.50E+01 | 9.50E+01 | 9.50E+01 |
| 6 | 0.54 | 185 | 608.7 | 913 | 0 | 1217.4 | 304.3 | -53.3 | -79.9 | 0 | -106.5 | -26.6 | 6 | 6 | 6 | 6 | 6 | 6.17E+03 | 6.17E+03 | 6.17E+03 | 6.17E+03 | 6.17E+03 | 1.30E+03 | 1.30E+03 | 1.30E+03 | 1.30E+03 | 1.30E+03 | 2.46E+02 | 2.46E+02 | 2.46E+02 | 2.46E+02 | 2.46E+02 | 1.91E+02 | 1.91E+02 | 1.91E+02 | 1.91E+02 | 1.91E+02 |
| 7 | 0.63 | 185 | 608.7 | 913 | 0 | 1217.4 | 304.3 | -53.3 | -79.9 | 0 | -106.5 | -26.6 | 7 | 7 | 7 | 7 | 7 | 8.11E+03 | 8.11E+03 | 8.11E+03 | 8.11E+03 | 8.11E+03 | 1.60E+03 | 1.60E+03 | 1.60E+03 | 1.60E+03 | 1.60E+03 | 4.24E+02 | 4.24E+02 | 4.24E+02 | 4.24E+02 | 4.24E+02 | 3.15E+02 | 3.15E+02 | 3.15E+02 | 3.15E+02 | 3.15E+02 |
| 8 | 0.72 | 185 | 608.7 | 913 | 0 | 1217.4 | 304.3 | -53.3 | -79.9 | 0 | -106.5 | -26.6 | 8 | 8 | 8 | 8 | 8 | 1.02E+04 | 1.02E+04 | 1.02E+04 | 1.02E+04 | 1.02E+04 | 1.97E+03 | 1.97E+03 | 1.97E+03 | 1.97E+03 | 1.97E+03 | 6.55E+02 | 6.55E+02 | 6.55E+02 | 6.55E+02 | 6.55E+02 | 4.65E+02 | 4.65E+02 | 4.65E+02 | 4.65E+02 | 4.65E+02 |
| 9 | 0.81 | 185 | 608.7 | 913 | 0 | 1217.4 | 304.3 | -53.3 | -79.9 | 0 | -106.5 | -26.6 | 9 | 9 | 9 | 9 | 9 | 1.26E+04 | 1.26E+04 | 1.26E+04 | 1.26E+04 | 1.26E+04 | 2.43E+03 | 2.43E+03 | 2.43E+03 | 2.43E+03 | 2.43E+03 | 9.55E+02 | 9.55E+02 | 9.55E+02 | 9.55E+02 | 9.55E+02 | 6.50E+02 | 6.50E+02 | 6.50E+02 | 6.50E+02 | 6.50E+02 |
| 10 | 0.9 | 185 | 608.7 | 913 | 0 | 1217.4 | 304.3 | -53.3 | -79.9 | 0 | -106.5 | -26.6 | 10 | 10 | 10 | 10 | 10 | 1.48E+04 | 1.48E+04 | 1.48E+04 | 1.48E+04 | 1.48E+04 | 2.87E+03 | 2.87E+03 | 2.87E+03 | 2.87E+03 | 2.87E+03 | 1.30E+03 | 1.30E+03 | 1.30E+03 | 1.30E+03 | 1.30E+03 | 8.48E+02 | 8.48E+02 | 8.48E+02 | 8.48E+02 | 8.48E+02 |
| 11 | 0.99 | 185 | 608.7 | 913 | 0 | 1217.4 | 304.3 | -53.3 | -79.9 | 0 | -106.5 | -26.6 | 11 | 11 | 11 | 11 | 11 | 1.67E+04 | 1.67E+04 | 1.67E+04 | 1.67E+04 | 1.67E+04 | 3.24E+03 | 3.24E+03 | 3.24E+03 | 3.24E+03 | 3.24E+03 | 1.65E+03 | 1.65E+03 | 1.65E+03 | 1.65E+03 | 1.65E+03 | 1.04E+03 | 1.04E+03 | 1.04E+03 | 1.04E+03 | 1.04E+03 |
| 12 | 1.08 | 185 | 608.7 | 913 | 0 | 1217.4 | 304.3 | -53.3 | -79.9 | 0 | -106.5 | -26.6 | 12 | 12 | 12 | 12 | 12 | 1.79E+04 | 1.79E+04 | 1.79E+04 | 1.79E+04 | 1.79E+04 | 3.49E+03 | 3.49E+03 | 3.49E+03 | 3.49E+03 | 3.49E+03 | 1.97E+03 | 1.97E+03 | 1.97E+03 | 1.97E+03 | 1.97E+03 | 1.20E+03 | 1.20E+03 | 1.20E+03 | 1.20E+03 | 1.20E+03 |
| 13 | 1.17 | 185 | 608.7 | 913 | 0 | 1217.4 | 304.3 | -53.3 | -79.9 | 0 | -106.5 | -26.6 | 13 | 13 | 13 | 13 | 13 | 1.85E+04 | 1.85E+04 | 1.85E+04 | 1.85E+04 | 1.85E+04 | 3.59E+03 | 3.59E+03 | 3.59E+03 | 3.59E+03 | 3.59E+03 | 2.24E+03 | 2.24E+03 | 2.24E+03 | 2.24E+03 | 2.24E+03 | 1.32E+03 | 1.32E+03 | 1.32E+03 | 1.32E+03 | 1.32E+03 |
| 14 | 1.26 | 185 | 608.7 | 913 | 0 | 1217.4 | 304.3 | -53.3 | -79.9 | 0 | -106.5 | -26.6 | 14 | 14 | 14 | 14 | 14 | 1.82E+04 | 1.82E+04 | 1.82E+04 | 1.82E+04 | 1.82E+04 | 3.50E+03 | 3.50E+03 | 3.50E+03 | 3.50E+03 | 3.50E+03 | 2.37E+03 | 2.37E+03 | 2.37E+03 | 2.37E+03 | 2.37E+03 | 1.35E+03 | 1.35E+03 | 1.35E+03 | 1.35E+03 | 1.35E+03 |
| 15 | 1.35 | 185 | 608.7 | 913 | 0 | 1217.4 | 304.3 | -53.3 | -79.9 | 0 | -106.5 | -26.6 | 15 | 15 | 15 | 15 | 15 | 1.78E+04 | 1.78E+04 | 1.78E+04 | 1.78E+04 | 1.78E+04 | 3.38E+03 | 3.38E+03 | 3.38E+03 | 3.38E+03 | 3.38E+03 | 2.48E+03 | 2.48E+03 | 2.48E+03 | 2.48E+03 | 2.48E+03 | 1.37E+03 | 1.37E+03 | 1.37E+03 | 1.37E+03 | 1.37E+03 |
| 16 | 1.44 | 185 | 608.7 | 913 | 0 | 1217.4 | 304.3 | -53.3 | -79.9 | 0 | -106.5 | -26.6 | 16 | 16 | 16 | 16 | 16 | 1.70E+04 | 1.70E+04 | 1.70E+04 | 1.70E+04 | 1.70E+04 | 3.19E+03 | 3.19E+03 | 3.19E+03 | 3.19E+03 | 3.19E+03 | 2.51E+03 | 2.51E+03 | 2.51E+03 | 2.51E+03 | 2.51E+03 | 1.35E+03 | 1.35E+03 | 1.35E+03 | 1.35E+03 | 1.35E+03 |
| 17 | 1.53 | 185 | 608.7 | 913 | 0 | 1217.4 | 304.3 | -53.3 | -79.9 | 0 | -106.5 | -26.6 | 17 | 17 | 17 | 17 | 17 | 1.62E+04 | 1.62E+04 | 1.62E+04 | 1.62E+04 | 1.62E+04 | 2.99E+03 | 2.99E+03 | 2.99E+03 | 2.99E+03 | 2.99E+03 | 2.51E+03 | 2.51E+03 | 2.51E+03 | 2.51E+03 | 2.51E+03 | 1.30E+03 | 1.30E+03 | 1.30E+03 | 1.30E+03 | 1.30E+03 |
| 18 | 1.62 | 185 | 608.7 | 913 | 0 | 1217.4 | 304.3 | -53.3 | -79.9 | 0 | -106.5 | -26.6 | 18 | 18 | 18 | 18 | 18 | 1.57E+04 | 1.57E+04 | 1.57E+04 | 1.57E+04 | 1.57E+04 | 2.87E+03 | 2.87E+03 | 2.87E+03 | 2.87E+03 | 2.87E+03 | 2.51E+03 | 2.51E+03 | 2.51E+03 | 2.51E+03 | 2.51E+03 | 1.29E+03 | 1.29E+03 | 1.29E+03 | 1.29E+03 | 1.29E+03 |
| 19 | 1.71 | 185 | 608.7 | 913 | 0 | 1217.4 | 304.3 | -53.3 | -79.9 | 0 | -106.5 | -26.6 | 19 | 19 | 19 | 19 | 19 | 1.49E+04 | 1.49E+04 | 1.49E+04 | 1.49E+04 | 1.49E+04 | 2.67E+03 | 2.67E+03 | 2.67E+03 | 2.67E+03 | 2.67E+03 | 2.52E+03 | 2.52E+03 | 2.52E+03 | 2.52E+03 | 2.52E+03 | 1.27E+03 | 1.27E+03 | 1.27E+03 | 1.27E+03 | 1.27E+03 |
| 20 | 1.8 | 185 | 608.7 | 913 | 0 | 1217.4 | 304.3 | -53.3 | -79.9 | 0 | -106.5 | -26.6 | 20 | 20 | 20 | 20 | 20 | 1.44E+04 | 1.44E+04 | 1.44E+04 | 1.44E+04 | 1.44E+04 | 2.53E+03 | 2.53E+03 | 2.53E+03 | 2.53E+03 | 2.53E+03 | 2.52E+03 | 2.52E+03 | 2.52E+03 | 2.52E+03 | 2.52E+03 | 1.26E+03 | 1.26E+03 | 1.26E+03 | 1.26E+03 | 1.26E+03 |
| 21 | 1.89 | 185 | 608.7 | 913 | 0 | 1217.4 | 304.3 | -53.3 | -79.9 | 0 | -106.5 | -26.6 | 21 | 21 | 21 | 21 | 21 | 1.40E+04 | 1.40E+04 | 1.40E+04 | 1.40E+04 | 1.40E+04 | 2.41E+03 | 2.41E+03 | 2.41E+03 | 2.41E+03 | 2.41E+03 | 2.51E+03 | 2.51E+03 | 2.51E+03 | 2.51E+03 | 2.51E+03 | 1.25E+03 | 1.25E+03 | 1.25E+03 | 1.25E+03 | 1.25E+03 |
| 22 | 1.98 | 185 | 608.7 | 913 | 0 | 1217.4 | 304.3 | -53.3 | -79.9 | 0 | -106.5 | -26.6 | 22 | 22 | 22 | 22 | 22 | 1.36E+04 | 1.36E+04 | 1.36E+04 | 1.36E+04 | 1.36E+04 | 2.30E+03 | 2.30E+03 | 2.30E+03 | 2.30E+03 | 2.30E+03 | 2.50E+03 | 2.50E+03 | 2.50E+03 | 2.50E+03 | 2.50E+03 | 1.25E+03 | 1.25E+03 | 1.25E+03 | 1.25E+03 | 1.25E+03 |
| 23 | 2.07 | 185 | 608.7 | 913 | 0 | 1217.4 | 304.3 | -53.3 | -79.9 | 0 | -106.5 | -26.6 | 23 | 23 | 23 | 23 | 23 | 1.33E+04 | 1.33E+04 | 1.33E+04 | 1.33E+04 | 1.33E+04 | 2.20E+03 | 2.20E+03 | 2.20E+03 | 2.20E+03 | 2.20E+03 | 2.48E+03 | 2.48E+03 | 2.48E+03 | 2.48E+03 | 2.48E+03 | 1.24E+03 | 1.24E+03 | 1.24E+03 | 1.24E+03 | 1.24E+03 |
| 24 | 2.16 | 185 | 608.7 | 913 | 0 | 1217.4 | 304.3 | -53.3 | -79.9 | 0 | -106.5 | -26.6 | 24 | 24 | 24 | 24 | 24 | 1.31E+04 | 1.31E+04 | 1.31E+04 | 1.31E+04 | 1.31E+04 | 2.11E+03 | 2.11E+03 | 2.11E+03 | 2.11E+03 | 2.11E+03 | 2.46E+03 | 2.46E+03 | 2.46E+03 | 2.46E+03 | 2.46E+03 | 1.23E+03 | 1.23E+03 | 1.23E+03 | 1.23E+03 | 1.23E+03 |
| 25 | 2.25 | 185 | 608.7 | 913 | 0 | 1217.4 | 304.3 | -53.3 | -79.9 | 0 | -106.5 | -26.6 | 25 | 25 | 25 | 25 | 25 | 1.28E+04 | 1.28E+04 | 1.28E+04 | 1.28E+04 | 1.28E+04 | 1.55E+03 | 1.55E+03 | 1.55E+03 | 1.55E+03 | 1.55E+03 | 2.44E+03 | 2.44E+03 | 2.44E+03 | 2.44E+03 | 2.44E+03 | 1.22E+03 | 1.22E+03 | 1.22E+03 | 1.22E+03 | 1.22E+03 |

# 3 Maps of wind, load and energy

## 3.1 EWTW - Predictions and comparison with measured data

### *3.1.1 Wind turbine model and measured data*

The wind turbine model consists of the thrust curve, which relates thrust coefficient $c_T$ to tip-speed ratio $\lambda$ (see section 2.2). Figure 9 shows the thrust curve of the wind turbines in the EWTW as obtained form public information (pages 109 and 131, Bundesverband WindEnergie, 2007). Note this thrust curve is an effective thrust curve in the sense of the discussion in section 2.2 as it includes the effect of the variation of the rotor speed between 10.9 rpm and 19.1 rpm. Also shown in figure 9 are the power curve from the same source and the power curve which originates from the parameterized thrust curve. Apart from the obviously erroneous point near a wind speed of 21 m/s the difference between the published and the modelled power curve is less than 4%.

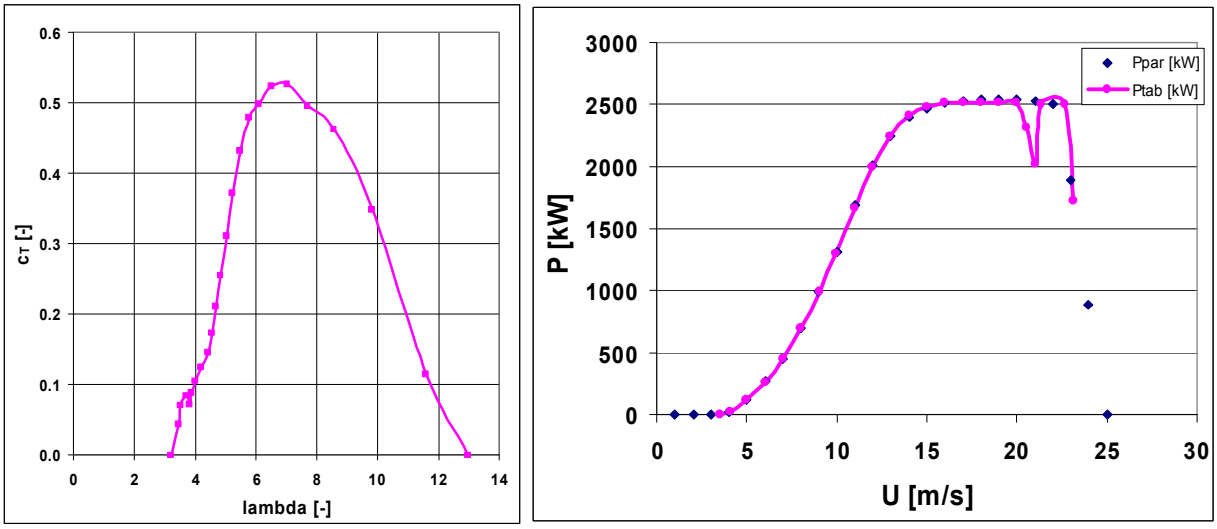


Figure 9 *Model of the wind turbines in the EWTW in the form of the published thrust curve (left) and the resulting power curve $P_{par}$ compared to the published power curve $P_{tab}$ (right); Source: Bundesverband WindEnergie 2007. The erroneous point at $\lambda = 3.8$ is excluded from the analysis*

The measured (confidential and restricted) data originate from the database at the dedicated ftp site at ECN (aeolus@ftp.ecn.nl) that was prepared as deliverable D1.1 in the project Aeolus. The data are described in more detail in appendix D and in Brand et al., 2008.

### *3.1.2 Inflow perpendicular to turbine row (case wd2)*

In this section inflow perpendicular to the row of turbines together with four wind speed cases is considered. (See figure D.1 for a definition sketch.) This wind direction case is relevant because it shows to what extent the state of each turbine is predicted if all turbines have the same inflow. The wind speed cases are relevant because they correspond to near cut-in (ws1), halfway nominal power (ws2), near nominal power (ws3) and constant power (ws4). The wind speed cases have been set on basis of the 10-minute averaged wind speed as measured at the meteo mast and correspond to an upstream turbulence intensity of the order of 10%. Figures 10, 11 and 12 show a comparison between calculated and measured mean values and figures 13, 14 and 15 show a comparison between calculated and measured standard deviations.

First it should be noted that even over the small separation distances in the EWTW there is some spatial variation in the mean inflow wind speed. For example, there are differences of the order of 1 m/s between the mean wind speed at the meteo mast and the individual wind turbines (figure 10) and even larger differences between the wind speed standard

deviations (figure 13). As another example all wind speeds at the high wind speed case (ws4) should be equal to the meteo mast reading 17-18 m/s, but in fact vary between 16 m/s and 18 m/s. These variations, which have not been taken into account in the modelling, cause variations in calculated power between the wind turbines, and to a smaller extent in tower bending moment and blade bending moment.

In addition there is a clear variation in standard deviation of inflow wind speed, which variation comes from the IJsselmeer where turbulence intensity is lower than over land. Nevertheless calculated standard deviations are of the correct order of magnitude.

### *3.1.3 Inflow aligned with turbine row (case wd1)*

In this section inflow aligned with the row of turbines together with four wind speed cases is considered; see figure D.1. This wind direction case is relevant because it shows to what extent the state of each turbine is predicted if all but one turbine is in the wake of another turbine. Again the wind speed cases have been set on basis of the 10-minute averaged wind speed as measured at the meteo mast and correspond to an upstream turbulence intensity of the order of 10%. Figures 16 to 21 show the various quantities as a function of the distance along the row of turbines, plus, in the case of wind speed, the upstream wind speed as measured at the meteo mast(s).

First it is checked whether the upstream wind turbine (T1) has the same inflow as the meteo mast (T0). This is the case for mean wind speed (figure 16), but not for wind speed standard deviation as there are differences up to 1 m/s (figure 19). The latter hampers an assessment of the supposed breakdown of the modelled impact of turbulence.

Figures 16, 17 and 18 compare calculated and measured 10-minute mean values. Here it is found that, apart from the high wind speed case, predicted mean wind speed in the wake is within a meter per second of measured wind speed. On the other hand predicted decay of wind speed deficit is too gradual, and measured wind speed minimum at second or third turbine is not calculated. This picture also emerges form power, tower bending moment, and blade bending moment.

Figures 19, 20 and 21 compare calculated and measured 10-minute standard deviations. As to calculated and measured wind speed standard deviation it must be noted that these can not be compared because the latter is measured at the hub, in the centre of the rotor disc. Anyway, although there is a reasonable but not good agreement for power of some of the turbines, the agreement is poor for power of the other turbines and for all bending moments. In general, turbulence is found to decay too fast.

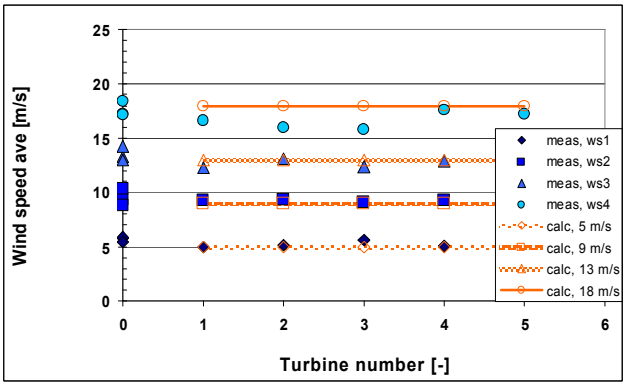


Figure 10 *Mean wind speed from the flow map of the EWTW plus the corresponding measured data; four wind speed cases; inflow perpendicular to turbine row. Turbine #0 indicates a meteo mast. Connecting lines are visual aids which connect markers but do not present calculated results*

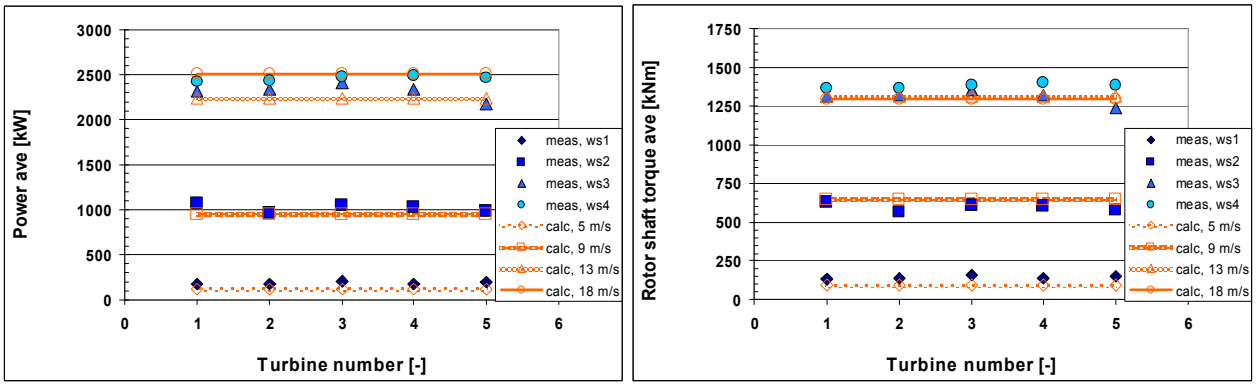


Figure 11 *Mean power (left) and rotor shaft torque (right) from the load/energy map of the EWTW plus the corresponding measured data for the four wind speed cases; inflow perpendicular to turbine row. Connecting lines are visual aids which connect markers but do not present calculated results*

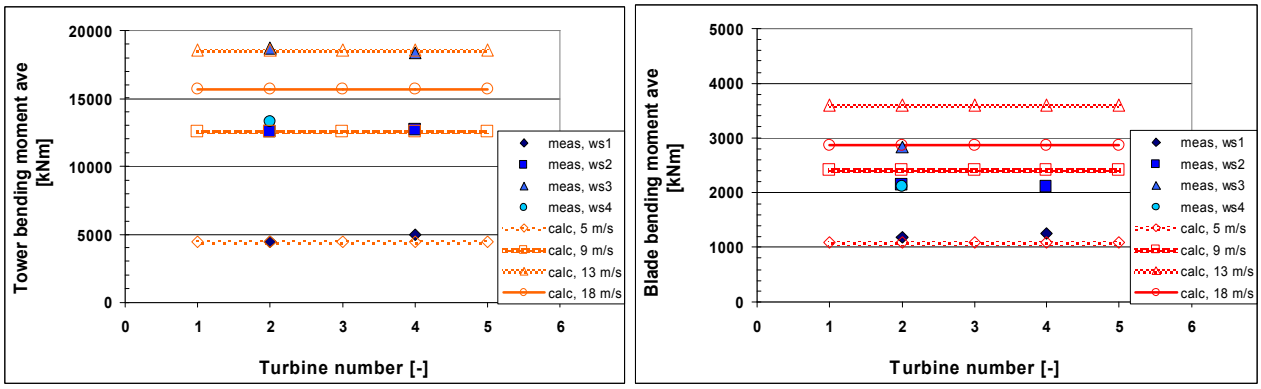


Figure 12 *Mean tower bending moment (left) and blade 1 bending moment (right) from the load map of the EWTW plus the corresponding measured data for the four wind speed cases; inflow perpendicular to turbine row. Connecting lines are visual aids which connect markers but do not present calculated results*

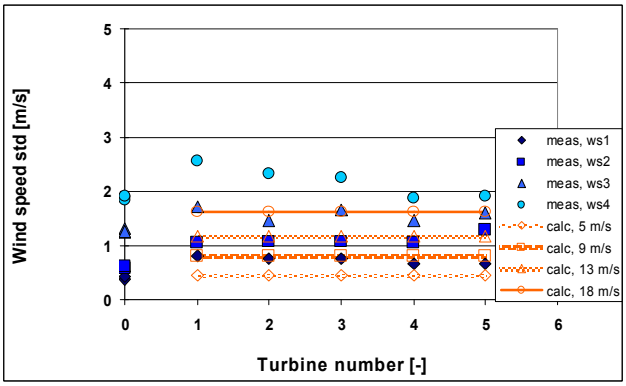


Figure 13 *Standard deviation of wind speed from the flow map of the EWTW plus the corresponding measured data; four wind speed cases; inflow perpendicular to turbine row. Turbine #0 indicates a meteo mast. Connecting lines are visual aids which connect markers but do not present calculated results*

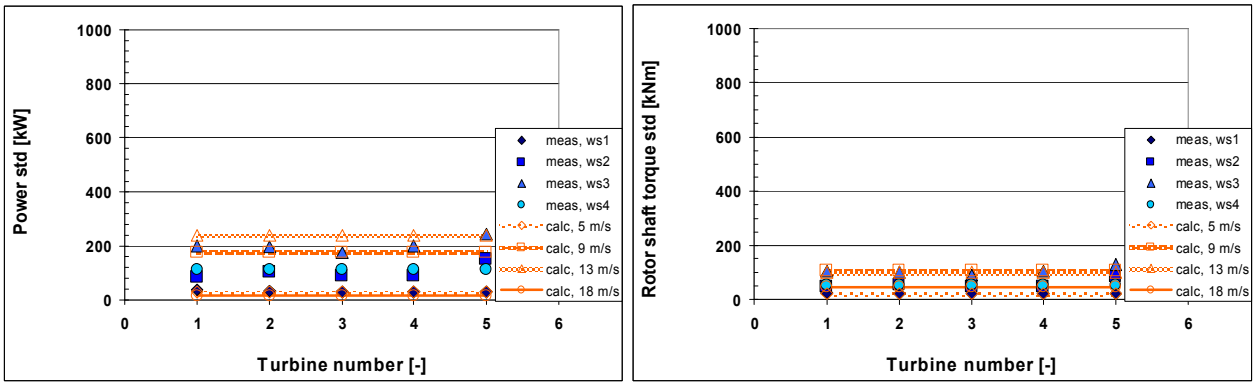


Figure 14 *Standard deviation of power (left) and rotor shaft torque (right) from the load/energy map of the EWTW plus the corresponding measured data for the four wind speed cases; inflow perpendicular to turbine row. Connecting lines are visual aids which connect markers but do not present calculated results*

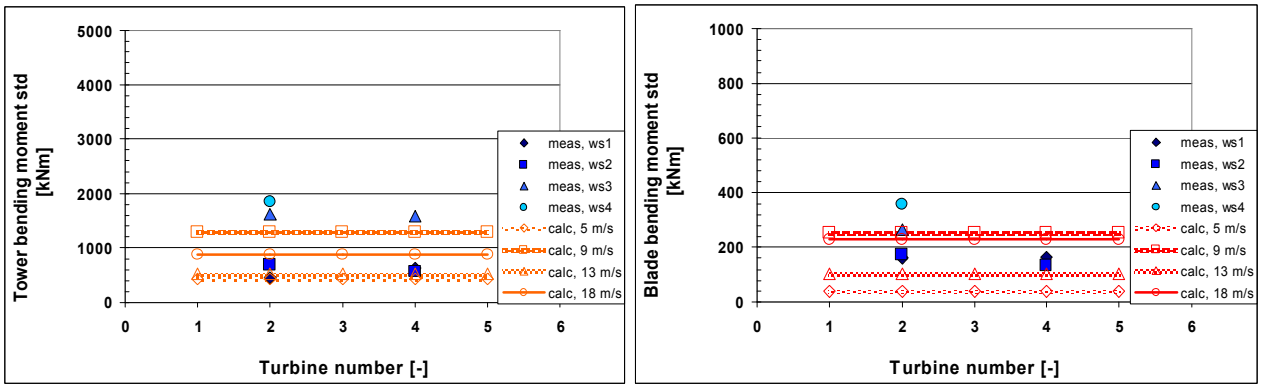


Figure 15 *Standard deviation of tower bending moment (left) and blade 1 bending moment (right) from the load map of the EWTW plus the corresponding measured data for the four wind speed cases; inflow perpendicular to turbine row. Connecting lines are visual aids which connect markers but do not present calculated results*

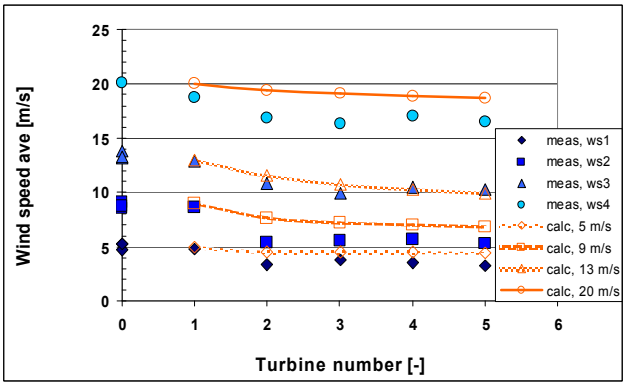


Figure 16 *Mean wind speed from the flow map of the EWTW plus the corresponding measured data; four wind speed cases cases; inflow aligned with turbine row. Turbine #0 indicates a meteo mast. Connecting lines are visual aids which connect markers but do not present calculated results*

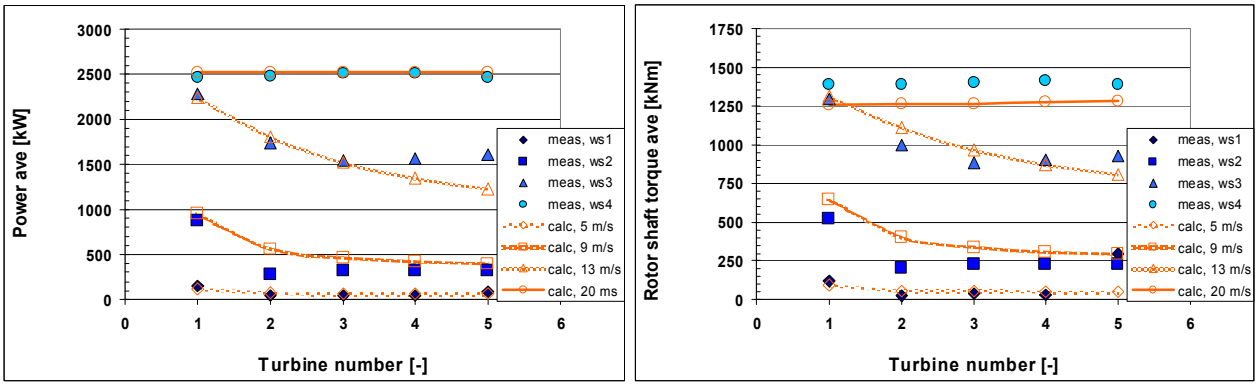


Figure 17 *Mean power (left) and rotor shaft torque (right) from the load/energy map of the EWTW plus the corresponding measured data for the four wind speed cases; inflow aligned with turbine row. Connecting lines are visual aids which connect markers but do not present calculated results*

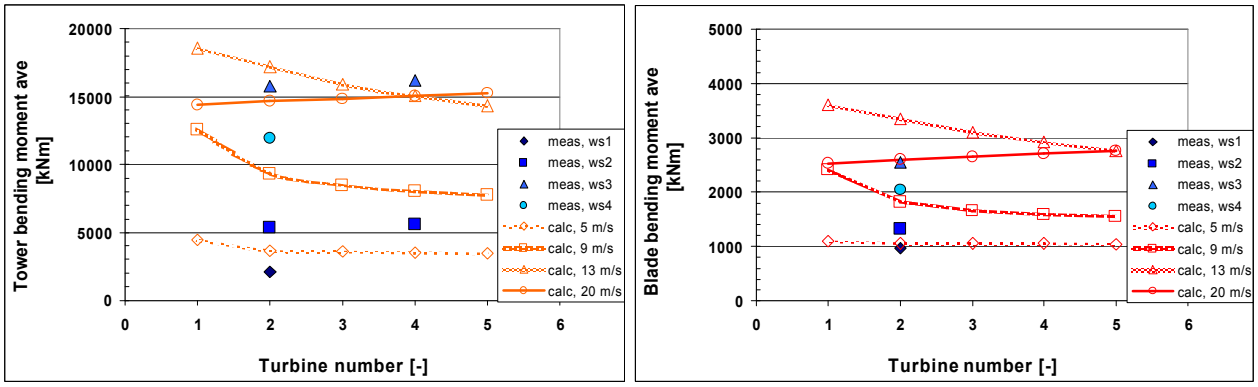


Figure 18 *Mean tower bending moment (left) and blade 1 bending moment (right) from the load map of the EWTW plus the corresponding measured data for the four wind speed cases; inflow aligned with turbine row. Connecting lines are visual aids which connect markers but do not present calculated results*

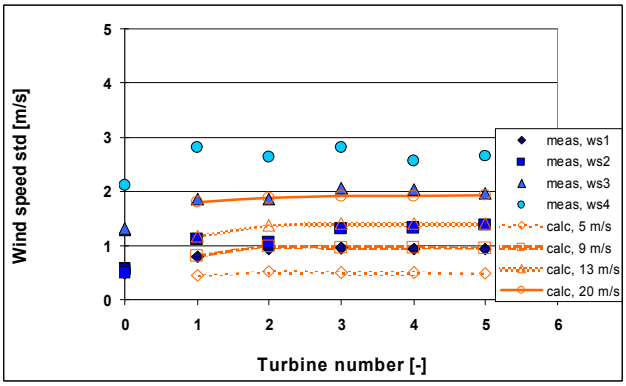


Figure 19 *Standard deviation of wind speed from the flow map of the EWTW plus the corresponding measured data; four wind speed cases; inflow aligned with turbine row. Turbine #0 indicates a meteo mast. Connecting lines are visual aids which connect markers but do not present calculated results*

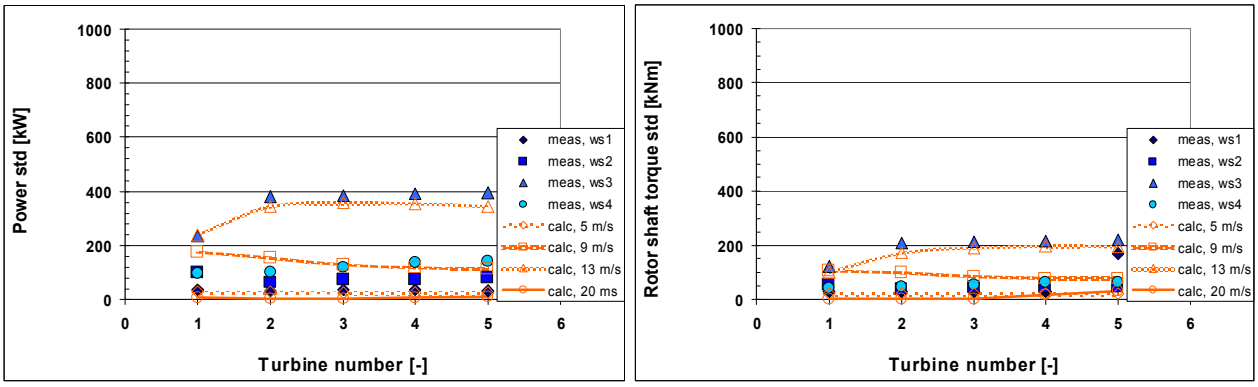


Figure 20 *Standard deviation of power (left) and rotor shaft torque (right) from the load/energy map of the EWTW plus the corresponding measured data for the four wind speed cases; inflow aligned with turbine row. Connecting lines are visual aids which connect markers but do not present calculated results*

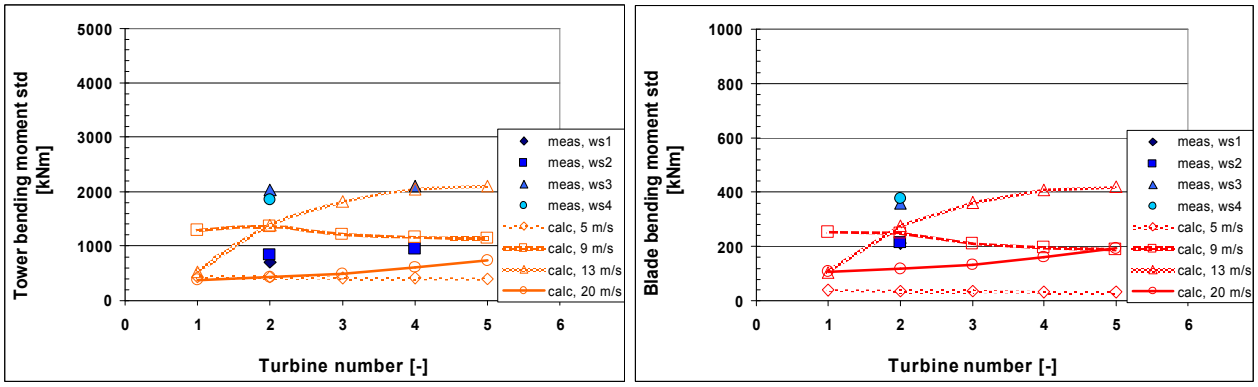


Figure 21 *Standard deviation of tower bending moment (left) and blade 1 bending moment (right) from the load map of the EWTW plus the corresponding measured data for the four wind speed cases; inflow aligned with turbine row. Connecting lines are visual aids which connect markers but do not present calculated results*

## 3.2 EWTW - Demonstration of power and short-term load quantifiers

In this section power and three short-term load quantifiers, as calculated by the quasi-steady flow model, are presented for the cases introduced in section 3.1. The motivation is that these quantities, together with for example rotor speed and blade pitch angle, are the primary quantities that are considered by a supervisory control algorithm. The short-term load quantifiers are equivalent tower bending moment (m=4), equivalent blade bending moment (m=12), and equivalent rotor-shaft torque (m=3).

Figure 22 shows calculated power and calculated load quantifiers as a function of wind speed in the case of inflow perpendicular to the row of five wind turbines in the EWTW. Clearly, since all turbines have the same inflow (mean wind speed and turbulence intensity of 9%), options to control the wind farm via the turbine wakes under these conditions are few.

Figure 23, on the other hand, shows that power and load quantifiers differ between the individual wind turbines when the inflow is along the row of wind turbines. This illustrates the options to control power of and loads in the wind farm via the wakes of the turbines. Note however that in this case the coupling via the wakes is strong because of the short distance of 3.8 rotor diameters between the turbines in the EWTW.

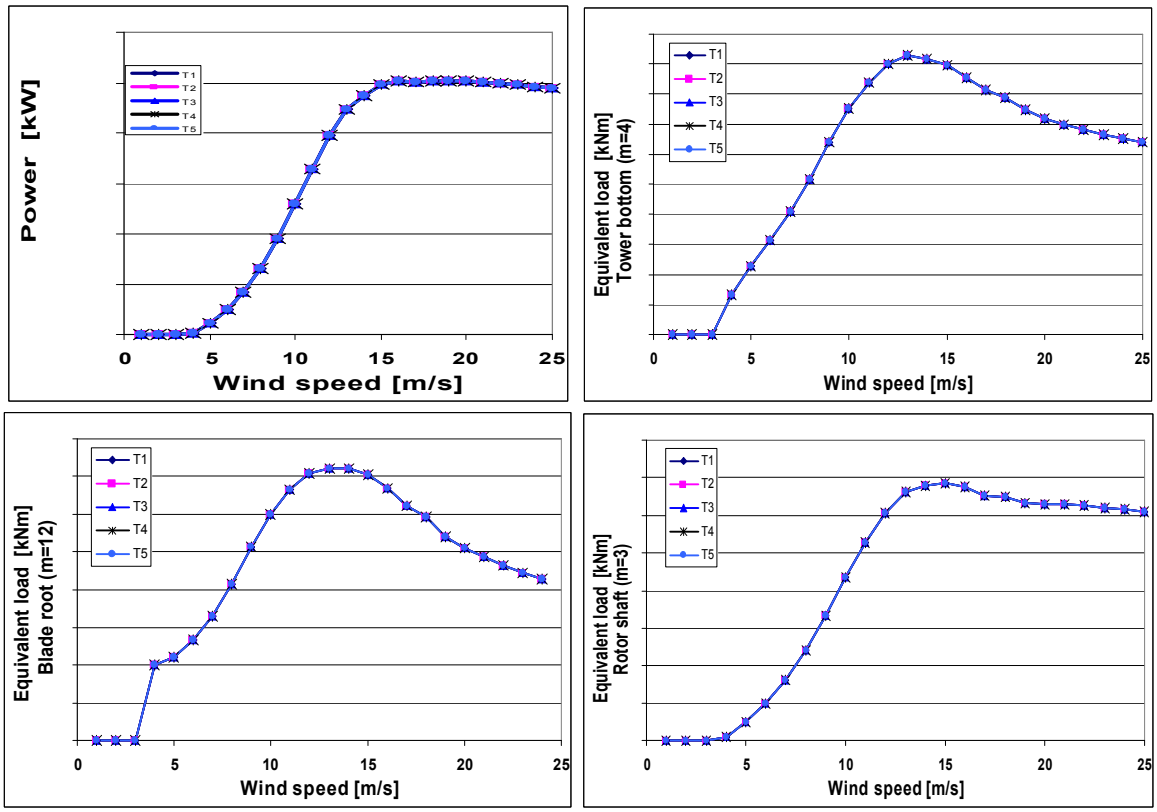


Figure 22 *Calculated power and load quantifiers for the turbine tower, the blade and the rotor shaft as a function of wind speed in the case of inflow perpendicular to the row of five wind turbines and a turbulence intensity of 9%*

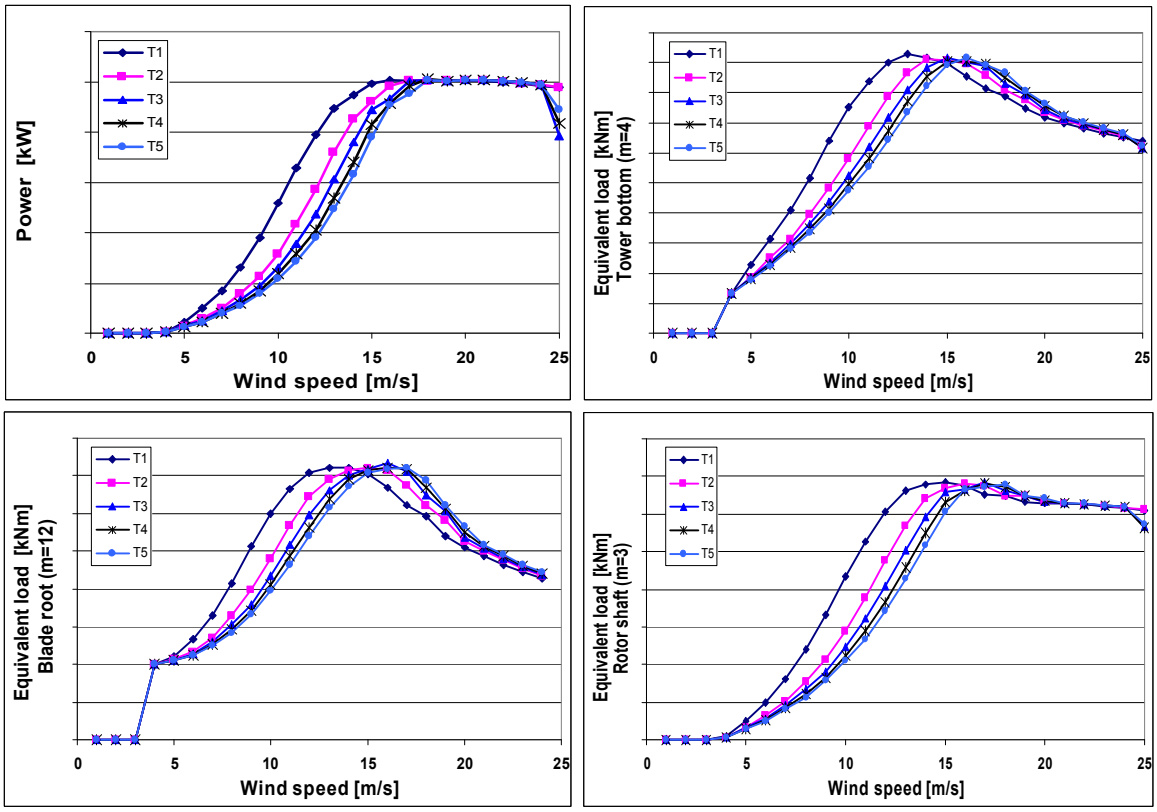


Figure 23 *Calculated power and load quantifiers for the turbine tower, the rotor blade and the rotor shaft as a function of wind speed in the case of inflow aligned with the row of five wind turbines and a turbulence intensity of 9%*

## 3.3 ESWF Predictions

### *3.3.1 Wind turbine model and measured data*

Figure 24 shows the thrust curve of the wind turbines in the ESWF as estimated from public data (Brand and Wagenaar, 2010). Note this thrust curve is an effective thrust curve in the sense of the discussion in section 2.2 as it includes the effect of variation of the rotor speed between 10.9 rpm and 19.1 rpm. Also shown in figure 24 are the power curve from the same source and the power curve which originates from the parameterized thrust curve.

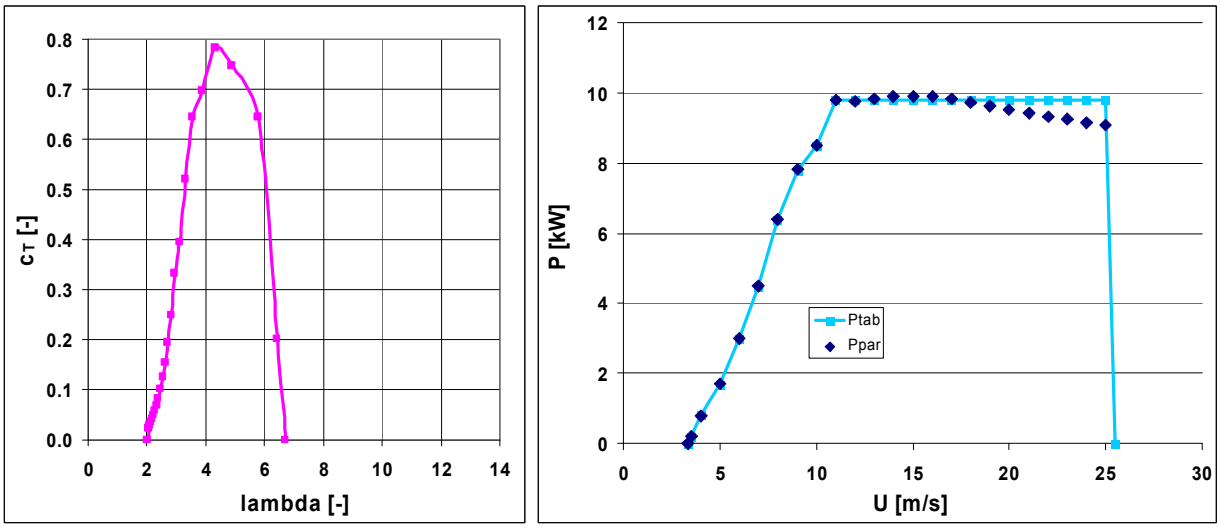


Figure 24 *Model of the wind turbines in the ESWF in the form of the estimated thrust curve (left), and the resulting power curve $P_{par}$ compared to the published power curve $P_{tab}$ (right)*

### *3.3.2 Inflow perpendicular to turbine row (case wd3)*

In this section inflow perpendicular to the row of turbines T1-T3-T6-T10 together with four wind speed cases is considered. (See figure E.1 for a definition sketch.) This wind direction is relevant because no wind turbine is in the wake of another wind turbine. Figure 25 shows that calculated variation between wind speed at and power of the various wind turbines is small indeed.

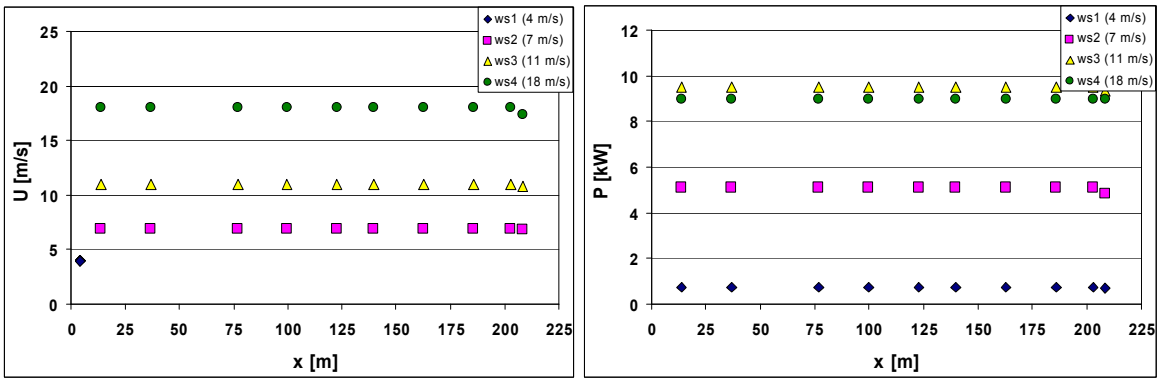


Figure 25 *Mean wind speed (left) and power (right) from the wind/power map of the ESWF for the four wind speed cases; inflow perpendicular to the row of turbines T1-T3-T6-T10. The x-coordinate indicates the turbine positions*

### 3.3.3 *Inflow aligned with turbine row (case wd1)*

In this section inflow aligned with three turbine rows is considered in combination with the four wind speed cases: T1-T3-T6-T10, T2-T4-T7 and T5-T9. (See figure E.1 for a definition sketch.) This wind direction case is relevant because some turbines are in the wake of another turbine, and some even in a multiple wake. Figure 26 shows the resulting variation in wind speed and power in the wind farm.

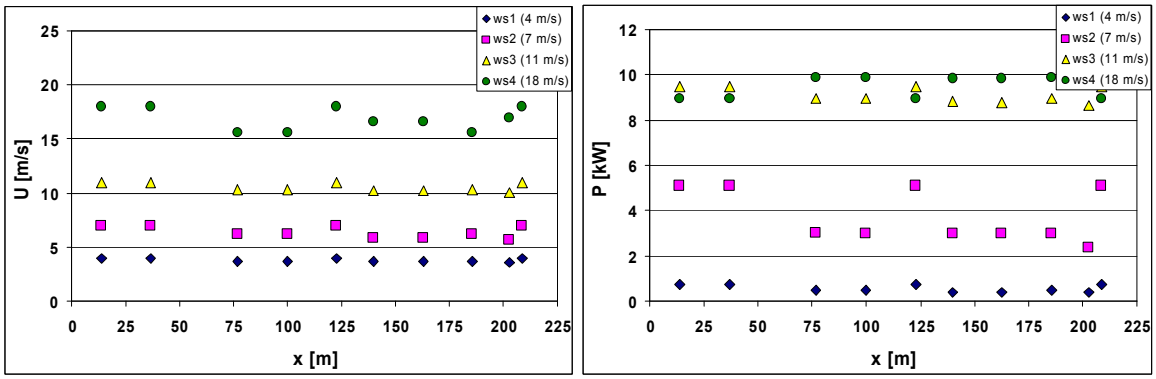


Figure 26 *Mean wind speed (left) and power (right) from the wind/power map of the ESWF for the four wind speed cases; inflow aligned with turbine rows T1-T3-T6-T10, T2-T4-T7 and T5-T9. The x-coordinate indicates the turbine positions*

### 3.3.4 *Inflow aligned with turbine row (case wd2)*

In this section inflow aligned with three turbine rows is considered in combination with the four wind speed cases: T1-T2, T3-T4-T5 and T6-T7-T8-T9. (See figure E.1 for a definition sketch.) Figure 27 shows the resulting variation in wind speed and power in the wind farm.

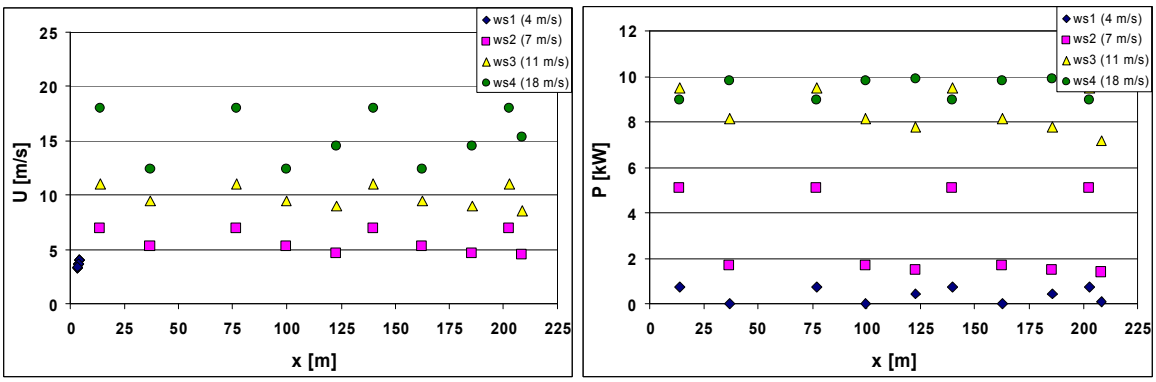


Figure 27 *Mean wind speed (left) and power (right) from the wind/power map of the ESWF for the four wind speed cases; inflow aligned with turbine rows T1-T2, T3-T4-T5 and T6-T7-T8-T9. The x-coordinate indicates the turbine positions*

### *3.3.5 Inflow aligned with turbine row (case wd4)*

In this section inflow aligned with three turbine rows is considered in combination with the four wind speed cases: T3-T2, T6-T4 and T10-T7-T5. (See figure E.1 for a definition sketch.) Figure 28 shows the resulting variation in wind speed and power in the wind farm.

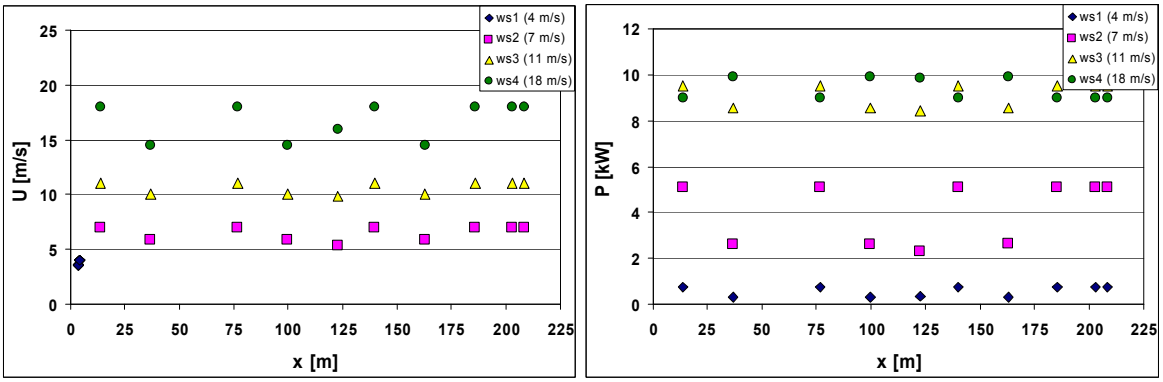


Figure 28 *Mean wind speed (left) and power (right) from the wind/power map of the ESWF for the four wind speed cases; inflow aligned with turbine rows T3-T2, T6-T4 and T10-T7-T5. The x-coordinate indicates the turbine positions*

# 4 Summary

Maps of wind, loads and energy have been presented for the ECN Wind turbine Test site Wieringermeer EWTW and the ECN Scale Wind Farm ESWF. These maps include tables with mean and standard deviation of

- Six quantities (wind speed at the turbine, rotor thrust, tower bending moment, blade bending moment, aerodynamic power, and rotor shaft torque) and
- Three short-term load quantifiers (equivalent tower bending moment, equivalent blade bending moment, and equivalent rotor shaft torque);
- Both as a function of three input quantities (mean wind speed, wind speed standard deviation, and wind direction).

In addition the approach and a computer programme that allows one to calculate these tables have been presented, and, for the EWTW, a comparison between the calculated maps and measured information.

It is concluded that differences between measurement and prediction are smaller than 2 m/s (wind speed) and 200 kW (power), measured minimum in wind speed and aerodynamic power at second or third turbine is not predicted, and main differences originate from un-modelled spatial variations in wind speed and too gradually modelled decay of wind speed.

Although it is expected that better results on the mean values can be obtained by fine tuning the model parameters in order to reproduce the measured data, the results are the best that can be obtained with this computationally cheap and fast model. A further improvement of the standard deviations on the other hand is needed, but this requires measured data from the ESWF.

## References

M. Abramowitz and I.A. Stegun,
*Handbook of mathematical functions (10th ed.),*
National Bureau of Standards, Applied Mathematics Series 55, 1972

R. Barthelmie, G. Larsen, S. Pryor, H. Jørgensen, H. Bergström, M. Magnusson, W. Schlez, K. Rados, B. Lange, P. Vølund, S. Neckelmann, S. Mogensen, G. Schepers, T. Hegberg, and L. Folkerts,
*Efficient Development of Offshore Windfarms (ENDOW),*
Report Risø-R-1407(EN), 2003

A.J. Brand,
*Preliminary maps of wind fields and loads and energy*,
FP7-ICT STREP 224548 / Aeolus Deliverable D1.3. 2009

A.J. Brand,
*Final maps of wind fields and mechanical loads and energy output Part 2: Quasi-steady wind farm flow model - User's manual*,
FP7-ICT STREP 224548 / Aeolus Deliverable D1.5b. 2010 (draft)

A.J. Brand, J.P. Verhoef and T.S. Obdam,
*Relevant datasets extracted from EWTW database*,
FP7-ICT STREP 224548 / Aeolus Deliverable D1.1. 2008

A.J. Brand and J.W. Wagenaar,
*Measurement and control infrastructure at the ECN Scale Wind Farm ESWF in the context of the FP7 project Aeolus,*
FP7-ICT STREP 224548 / Aeolus Technical Report T1.5. 2010 (draft)

T. Burton, D. Sharp, N. Jenkins and E. Bossanyi,
*Handbook of Wind Energy*,
John Wiley and Sons, ISBN 0 471 48997 2, 2001

J.W.M. Dekker and J.T.G. Pierik (ed.),
*European Wind Turbine Standards II*,
ECN-C--99-073

D.L. Elliott,
*Status of wake and array loss research*,
In: Proc. Windpower91, Palm Springs, California, 24-27 September 1991

*Guidelines for Design of Wind Turbines (1st ed.),*
Det Norske Veritas and Risø National Laboratory, ISBN 87-550-2870-5, 2001

J.F. Manwell, J.G. McGowan and A.L. Rogers,
*Wind energy explained*,
John Wiley and Sons, ISBN 0 471 49972 2, 2002

D.J. Milborrow,
*The performance of arrays of wind turbines*,
J. Industrial Aerodynamics, 5 (1980), pp. 403-430

A.M. Mood, F.A. Graybill and D.C. Boes,
*Introduction to the theory of statistics (3rd ed.),*
McGraw-Hill, ISBN 0 07 042864 6, 1974

E.W. Weisstein,
*Gaussian Integral*,
From MathWorld - A Wolfram Web Resource, http://mathworld.wolfram.com/GaussianIntegral.html (4 March 2010)

*Wind energy market 2007/2008*,
Bundesverband WindEnergie e.v., ISBN 978 3 980 6657 5 9, 2007

# Appendix A Mean and variance of function of normally distributed variable

## A.1 Function of one variable

Consider the function f of the variable x where x has a normal distribution with mean $\mu_x$ and standard deviation $\sigma_x$:

$$y = f(x) \text{ with } x : N(\mu_x, \sigma_x)$$

Then from the Taylor series of f(x) it follows that y can be approximated by a normal distribution (see e.g. chapter V in Mood et. al):

$$y : N(\mu_y, \sigma_y) \text{ with } \mu_y \approx f(\mu_x) + \frac{1}{2}\sigma_x^2 \left.\frac{d^2 f}{dx^2}\right|_{\mu_x} \text{ and } \sigma_y^2 \approx \sigma_x^2 \left[ \left( \left.\frac{df}{dx}\right|_{\mu_x} \right)^2 + \frac{1}{2}\sigma_x^2 \left( \left.\frac{d^2 f}{dx^2}\right|_{\mu_x} \right)^2 \right]$$

## A.2 Function of two variables

Consider the function f of the two variables x and y where x has a normal distribution with mean $\mu_x$ and standard deviation $\sigma_x$ and y has a normal distribution with mean $\mu_y$ and standard deviation $\sigma_y$:

$$z = f(x, y) \text{ with } x : N(\mu_x, \sigma_x) \text{ and } y : N(\mu_y, \sigma_y)$$

Then from the Taylor series of f(x,y) it follows that z can be approximated by a normal distribution (see e.g. chapter V in Mood et al.):

$$z : N(\mu_z, \sigma_z)$$

with

$$\mu_z \approx f(\mu_x, \mu_y) + \frac{1}{2}\sigma_x^2 \left.\frac{d^2 f}{dx^2}\right|_{\mu_x,\mu_y} + c_{xy}\sigma_x\sigma_y \left.\frac{d^2 f}{dxdy}\right|_{\mu_x,\mu_y} + \frac{1}{2}\sigma_y^2 \left.\frac{d^2 f}{dy^2}\right|_{\mu_x,\mu_y}$$

and

$$\sigma_z^2 \approx \sigma_x^2 \left( \left.\frac{df}{dx}\right|_{\mu_x,\mu_y} \right)^2 + \sigma_y^2 \left( \left.\frac{df}{dy}\right|_{\mu_x,\mu_y} \right)^2 + \frac{1}{2}\sigma_x^4 \left( \left.\frac{d^2 f}{dx^2}\right|_{\mu_x,\mu_y} \right)^2 + \frac{1}{2}\sigma_y^4 \left( \left.\frac{d^2 f}{dy^2}\right|_{\mu_x,\mu_y} \right) + c_{xy}^2\sigma_x^2\sigma_y^2 \left.\frac{d^2 f}{dx^2}\right|_{\mu_x,\mu_y} \left.\frac{d^2 f}{dy^2}\right|_{\mu_x,\mu_y} +$$
$$(1 + c_{xy}^2)\sigma_x^2\sigma_y^2 \left( \left.\frac{d^2 f}{dxdy}\right|_{\mu_x,\mu_y} \right)^2 + 2c_{xy}\sigma_x\sigma_y \left( \left.\frac{df}{dx}\right|_{\mu_x,\mu_y} \left.\frac{df}{dy}\right|_{\mu_x,\mu_y} + \left.\frac{d^2 f}{dxdy}\right|_{\mu_x,\mu_y} \left( \sigma_x^2 \left.\frac{d^2 f}{dx^2}\right|_{\mu_x,\mu_y} + \sigma_y^2 \left.\frac{d^2 f}{dy^2}\right|_{\mu_x,\mu_y} \right) \right)$$

where $c_{xy}$ is the correlation coefficient of x and y.

## Appendix B Axial force on a rotor blade

If a, a' and λ are axial induction factor, tangential induction factor and tip speed ratio respectively, non-dimensional axial force $f_b$ on a rotor blade section is (e.g. section 3.3 in Burton et al.):

$$f_b^2 = f_{b,x}^2 + f_{b,y}^2 = \left(8\pi \frac{U^2}{W^2} \frac{R}{N_b c}\right)^2 \left[\left(a(1-a) + (\lambda a')^2\right)^2 + (\lambda a'(1-a))^2\right]$$

with

$$\frac{W^2}{U^2} = \frac{U^2(1-a)^2 + \Omega^2 R^2 (1+a')^2}{U^2} = (1-a)^2 + \lambda^2 (1+a')^2 \text{ and } a' = \frac{a(1-a)}{\lambda^2}$$

and where U is wind speed at hub height, W is effective wind speed at a rotor blade, R is length of the rotor blade, c is chord length of the rotor blade section and $N_b$ is number of rotor blades. Note $f_{b,x}$ and $f_{b,y}$ denote normal and tangential component of the non-dimensional force on a rotor blade section.

At a first approximation it can be shown that

$$f_b \approx \frac{8\pi R}{N_b c} \frac{a(1-a)}{\lambda^2}$$

from which it follows that axial force $F_b$ on a rotor blade is

$$F_b = \frac{1}{2} \rho W^2 f_b Rc \approx \frac{4\pi\rho\Omega^2 R^4}{N_b} \frac{a(1-a)}{\lambda^2}$$

## Appendix C Relation between power n and power m

When decaying, velocity deficit and added turbulence mix with the outer flow. Now consider the sum of energy in the mean and the turbulent velocity to be balanced by energy from the outer flow:

$$\frac{d\mu^2}{dx}+\frac{d\sigma^2}{dx}+\frac{dS}{dx}=0 \text{ with } \mu(x)=\left[1-\frac{\Delta\mu_{ini}}{\mu_0}\left(\frac{x}{2D}\right)^n\right]\mu_0 \text{ and } \sigma^2(x)=\sigma_0^2+\sigma_{add,ini}^2\left(\frac{x}{2D}\right)^m ;$$

and where $\frac{\Delta\mu_{ini}}{\mu_0}=2a$ according to momentum theory and $\frac{\sigma_{add,ini}^2}{\sigma_0^2}\propto a\frac{\mu_0^2}{\sigma_0^2}$ according to the CGL model.

Now assume that energy that is fed to the mean flow from the outer flow is a fraction k of the energy that is fed from the turbulent flow:

$$\frac{dS}{dx}=k\frac{d\sigma^2}{dx}.$$

Then it can be shown that power n and power m satisfy:

$$-2n\mu_0\Delta\mu_{ini}\left[1-\frac{\Delta\mu_{ini}}{\mu_0}\left(\frac{x}{2D}\right)^n\right]\left(\frac{x}{2D}\right)^n+m(1+k)\sigma_{add,ini}^2\left(\frac{x}{2D}\right)^m=0 .$$

For example at x= 2D we obtain:

$$m=\frac{4n}{1+k}\frac{\mu_0^2}{\sigma_0^2}(1-a)(1-2a).$$

## Appendix D Measured data EWTW

The measured data consist of 10-minute averaged quantities obtained under conditions where all 5 turbines in the ECN Wind turbine Test site Wieringermeer EWTW operated normally during approximately 1 hour at combinations of 4 wind speed ranges and 3 wind direction ranges (see figure D.1):

- Wind speed at hub height [m/s]:
  (1) 2 - 4 and 4 - 6 (near cut-in)
  (2) 8 - 10 (halfway nominal power)
  (3) 12 -14 (near nominal power)
  (4) 16 - 18 and 18 -20 (high wind speed)
- Wind direction at hub height [deg]:
  (1) 270 - 280 (aligned)
  (2) 180 - 190 (perpendicular)
  (3) 240 - 250 (misaligned)

These confidential and restricted data, which are available via a dedicated ftp site at ECN (aeolus@ftp.ecn.nl), are described in more detail in Brand et al., 2008.

These data originate from the 5 Nordex wind turbines (T5, T6, T7, T8 and T9) and the 3 meteo masts (MM1, MM2 and MM3) at the ECN wind turbine test field EWTW and were measured between 1 August 2005 and 30 April 2008. Data measured at the turbines include standard quantities (electrical power, blade pitch angle, rotor azimuth, generator speed and status), environmental quantities (wind speed and direction), and, at 2 turbines, mechanical quantities (like tower bending moments and blade root bending moments). Meteo data include wind speed, wind direction, and air temperature. Appendix A in Brand et al., 2008, gives a short description of the EWTW.

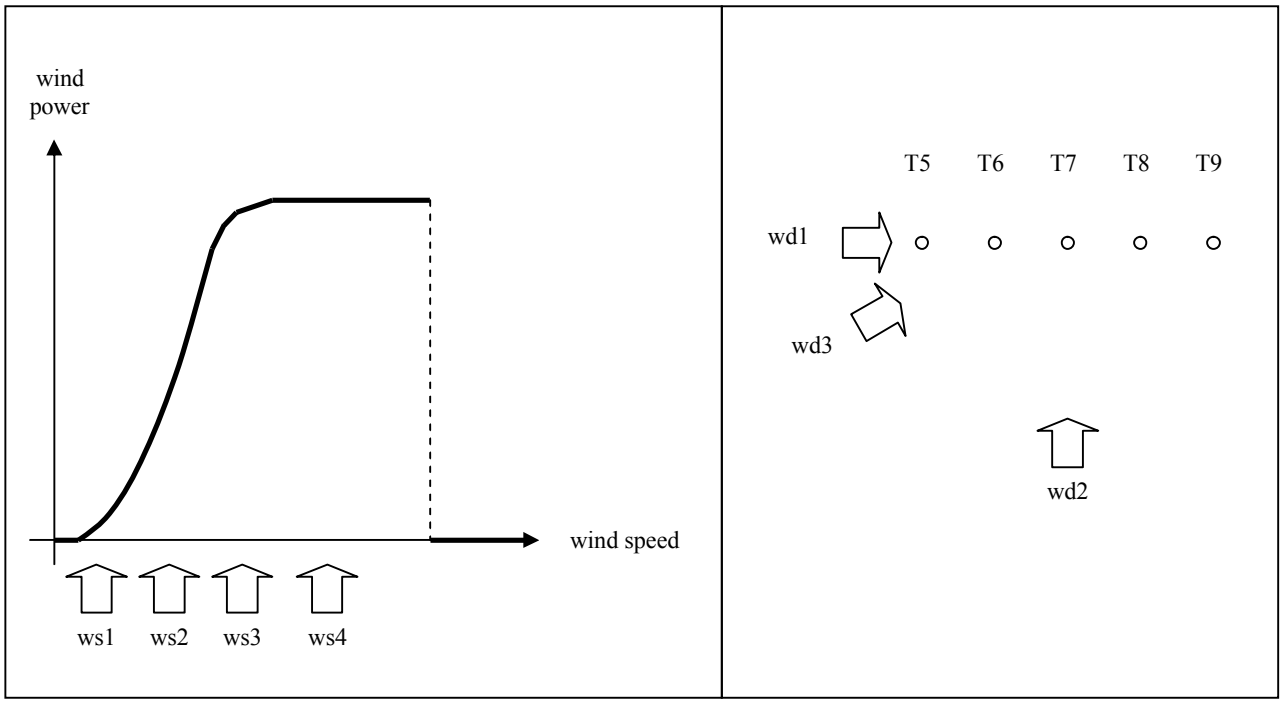


Figure D.1 *Description of the wind speed ranges (left) and the wind direction ranges (right) in the EWTW*

## Appendix E Data ESWF

It is planned to consider measured data consisting of 10-minute averaged quantities obtained under conditions where all 10 turbines in the ECN Scale Wind Farm ESWF operated normally during approximately 1 hour at combinations of 4 wind speed ranges and 4 wind direction ranges (see figure E.1):

- Wind speed at hub height [m/s]:
  (1) 4.0 ± 0.5 (near cut-in)
  (2) 7.0 ± 0.5 (halfway nominal power)
  (3) 11.0 ± 0.5 (near nominal power)
  (4) 18.0 ± 0.5 (high wind speed)
- Wind direction at hub height [deg]:
  (1) Aligned with row T1-T10, 270 ± 5
  (2) Aligned with row T6-T9, 235 ± 5
  (3) Perpendicular to row T1-T10, 180 ± 5
  (4) Aligned with row T5-T10, 112.5 ± 5.0

Brand and Wagenaar, 2010, gives a short description of the ESWF.

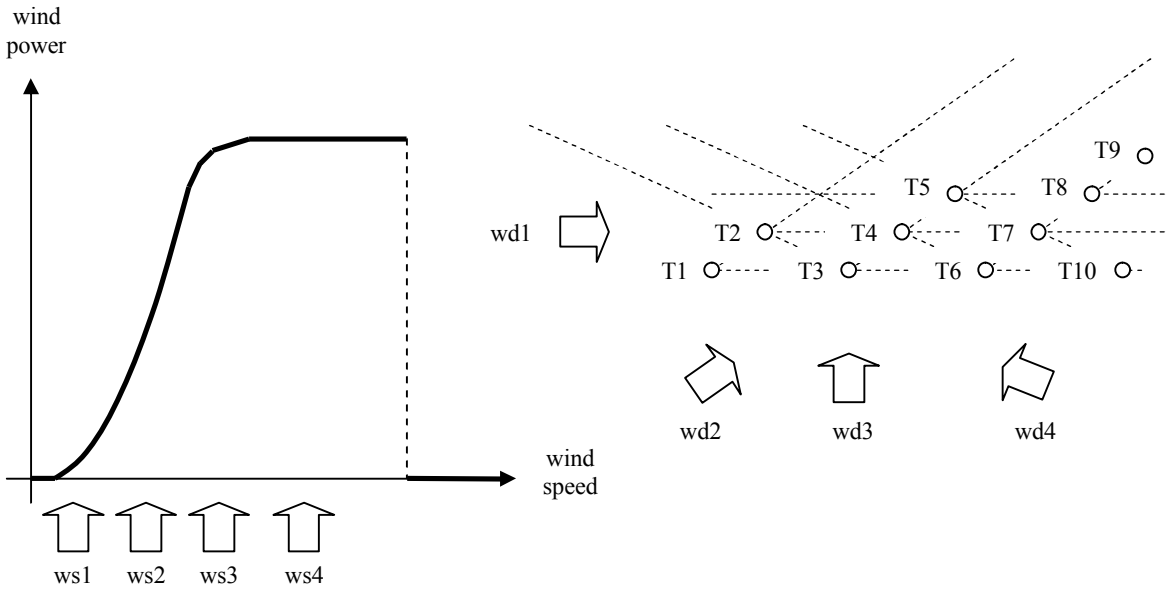


Figure E.1 *Description of the wind speed ranges (left) and the wind direction ranges (right) in the ESWF*